NASA Technical Paper 1169

Application of a Two-Dimensional Parabolic Computer Program to Prediction of Turbulent Reacting Flows

John S. Evans, Charles J. Schexnayder, Jr.,
and H. L. Beach, Jr.

MARCH 1978

NASA

NASA Technical Paper 1169

Application of a Two-Dimensional Parabolic Computer Program to Prediction of Turbulent Reacting Flows

John S. Evans, Charles J. Schexnayder, Jr.,
and H. L. Beach, Jr.
Langley Research Center
Hampton, Virginia

NASA
National Aeronautics
and Space Administration

Scientific and Technical
Information Office

1978

SUMMARY

The capabilities of a computer program obtained from the Spalding group at the Imperial College (London) and further developed by NASA are explored, and computed results are compared with data. The comparisons are restricted to two-dimensional (2-D) flows; that is, to mixing between parallel streams, plane or axisymmetric. Subsonic and supersonic flows, ducted and nonducted, reacting and nonreacting, are considered. Evaluation of models used for turbulence and chemical reaction form an important part of the study.

Constants in the $k - \varepsilon$ turbulence model, which produces mixing in good agreement with data, are the same for all calculations, but good initial profiles of turbulence kinetic energy k and dissipation rate of turbulence kinetic energy ε are necessary to obtain satisfactory results. To obtain agreement with data in reacting flows, adjustment is necessary over an order-of-magnitude range of a constant in the eddy-breakup reaction model. Since calculated results in agreement with the data can be obtained only by adjusting initial profiles in the $k - \varepsilon$ model and a parameter in the reaction model, a true predictive capability is not present. However, the program is useful for interpreting and extrapolating the results of experiments.

Experimental data were largely drawn from the literature, but new data are reported for coaxial injection at matched pressure (1 atm or 101.3 kPa) of a cold, Mach 2, hydrogen jet into a hot, Mach 2, vitiated airstream. Profiles of pitot pressure and gas composition obtained from water-cooled probes are reported and compared with theoretical results.

INTRODUCTION

A vital part of the effort (ref. 1) to develop a supersonic combustion ramjet engine (scramjet) is the capability for theoretical prediction of flow properties in the combustor, where hydrogen is injected into and burned in a supersonic airstream. For complete generality, the prediction method should be able to calculate turbulent mixing and chemical reaction in a combustor for arrays of hydrogen injectors at various angles to the airstream. The effects of the combustor walls on the flow should be included, and an ability to predict the effects of ignition sources and flame holders (in premixed flow) is needed. Shock waves and expansions must be accounted for.

Practical limitations of various kinds make difficult the inclusion of all these capabilities in a single program. The present program is restricted to mixing of parallel streams, subsonic or supersonic, plane or axisymmetric, reacting or nonreacting, ducted or nonducted. Since it is a two-dimensional program, three-dimensional effects such as injection from arrays or at angles to the flow are excluded. Interaction with walls is handled by using wall functions (ref. 2), a device which transmits the influence of a wall through the wall boundary layer

without calculating details of the wall boundary-layer flow. Turbulence is modeled using the $k - \varepsilon$ model (ref. 2) and chemical reaction is modeled using a modified form of the eddy breakup model (ref. 3).

Many reports have been published in which experimental mixing data for turbulent flows have been compared with predictions made by using finite-difference programs similar to the one described here. Some of these used the $k - \varepsilon$ turbulence model (or one of its "cousins" in which the dissipation rate ε is replaced with a frequency or a scale length). The collection of papers in reference 4 gives a representative sample of such work.

Few reports are available which give measured composition profiles in turbulent flames - especially for supersonic flow. Also, there are no satisfactory models available for theoretical calculation of chemical reaction in turbulent flows. Some new data on composition in a supersonic flame are published here, and emphasis is laid on testing the abilities of the chosen turbulence model and the chosen reaction model to predict the properties of turbulent reacting flow.

NOMENCLATURE

a	mass fraction
C_{EBU}	coefficient in eddy breakup model
$C_\mu, C_{\varepsilon 1}, C_{\varepsilon 2}, C_{g1}, C_{g2}$	coefficients in turbulence model
D	nozzle diameter, m
d_j	jet diameter, m
f	acceleration parameter in turbulence model
g	mean square fluctuation in mass fraction
h	slot height, m
$\hat{h}$	total enthalpy, m^2s^{-2}
i	parameter in transport equations
k	turbulence kinetic energy, m^2s^{-2}
ℓ_m	mixing length, m
ℓ_ε	characteristic length for dissipation of k, m
M	Mach number
m	mole fraction

p	static pressure, Pa
p_{ref}	reference pressure, Pa
$p_{t,2}$	pitot pressure, Pa
r	radius, m
r_1	upper limit of r for mass flow integral
T	temperature, K
u	flow velocity in principal flow direction, ms^{-1}
v	flow velocity in transverse direction, ms^{-1}
$\dot{w}$	chemical reaction rate, $kgm^{-3}s^{-1}$
x	distance along flow direction, m
y	distance normal to flow direction, m
ε	dissipation rate of turbulence kinetic energy, m^2s^{-3}
μ	viscosity, Nsm^{-2}
ρ	density, kgm^{-3}
σ	Prandtl number
τ	shear stress, Nm^{-2}

Subscripts:

cl	center line
e	edge
f	fuel
g	fluctuation
h	enthalpy
j	jet
k	turbulence kinetic energy
m	species
o	initial

ox	oxidant
t	turbulent
u	velocity in flow direction
ε	dissipation rate

Chemical notation:

Ar	argon
H_2	hydrogen
H_2O	water
N_2	nitrogen
O_2	oxygen

DESCRIPTION OF PROGRAM

The two-dimensional (2-D), parabolic computer program is described in references 5 and 6. It is basically the program the contractor delivered but has been tailored to fit the needs of the users. Solutions of parabolic partial differential equations for transport of momentum, energy, and mass are accomplished by the finite-difference technique of Patankar and Spalding (ref. 7). These equations are

$$\rho u \frac{\partial u}{\partial x} + \rho v \frac{\partial u}{\partial y} - \frac{1}{y^i} \frac{\partial}{\partial y}\left(\mu_t y^i \frac{\partial u}{\partial y}\right) = -\frac{dp}{dx} \tag{1}$$

$$\rho u \frac{\partial \hat{h}}{\partial x} + \rho v \frac{\partial \hat{h}}{\partial y} - \frac{1}{y^i} \frac{\partial}{\partial y}\left(\frac{\mu_t}{\sigma_h} y^i \frac{\partial \hat{h}}{\partial y}\right) = \frac{1}{y^i} \frac{\partial}{\partial y}\left\{y^i\left[\left(\frac{\mu_t}{\sigma_u} - \frac{\mu_t}{\sigma_h}\right)\frac{\partial}{\partial y}\left(\frac{u^2}{2}\right) + \left(\frac{\mu_t}{\sigma_k} - \frac{\mu_t}{\sigma_h}\right)\frac{dk}{dy}\right]\right\} \tag{2}$$

$$\rho u \frac{\partial a}{\partial x} + \rho v \frac{\partial a}{\partial y} - \frac{1}{y^i} \frac{\partial}{\partial y}\left(\frac{\mu_t}{\sigma_m} y^i \frac{\partial a}{\partial y}\right) = \dot{w} \tag{3}$$

where $i = 0$ for plane flow, and $i = 1$ for axisymmetric flow.

Two more equations are solved for the transport of turbulence kinetic energy k and of the dissipation rate of turbulence kinetic energy ε

$$\rho u \frac{\partial k}{\partial x} + \rho v \frac{\partial k}{\partial y} - \frac{1}{y^i} \frac{\partial}{\partial y}\left(\frac{\mu_t}{\sigma_k} y^i \frac{\partial k}{\partial y}\right) = \mu_t\left(\frac{\partial u}{\partial y}\right)^2 - \rho\varepsilon \tag{4}$$

$$\rho u \frac{\partial \varepsilon}{\partial x} + \rho v \frac{\partial \varepsilon}{\partial y} - \frac{1}{y^i} \frac{\partial}{\partial y}\left(\frac{\mu_t}{\sigma_\varepsilon} y^i \frac{\partial \varepsilon}{\partial y}\right) = C_{\varepsilon 1}\left(\frac{\varepsilon}{k}\right)\mu_t\left(\frac{\partial u}{\partial y}\right)^2 - C_{\varepsilon 2}\left(\frac{\varepsilon}{k}\right)\rho\varepsilon \tag{5}$$

Equations are also solved for the transport of fluctuations in fuel and oxidant.

$$\rho u \frac{\partial g_f}{\partial x} + \rho v \frac{\partial g_f}{\partial y} - \frac{1}{y^i} \frac{\partial}{\partial y}\left(\frac{\mu_t}{\sigma_g} \frac{\partial g_f}{\partial y}\right) = C_{g1}\left(\frac{\varepsilon}{k}\right)\left(\frac{\partial u}{\partial y}\right)^2 - C_{g2}\left(\frac{\varepsilon}{k}\right)\rho g_f \tag{6}$$

$$\rho u \frac{\partial g_{ox}}{\partial x} + \rho v \frac{\partial g_{ox}}{\partial y} - \frac{1}{y^i} \frac{\partial}{\partial y}\left(\frac{\mu_t}{\sigma_g} \frac{\partial g_{ox}}{\partial y}\right) = C_{g1}\left(\frac{\varepsilon}{k}\right)\left(\frac{\partial u}{\partial y}\right)^2 - C_{g2}\left(\frac{\varepsilon}{k}\right)\rho g_{ox} \tag{7}$$

Turbulence viscosity is computed from

$$\mu_t = \frac{C_\mu \rho k^2}{\varepsilon} \tag{8}$$

The chemical reaction rate[1] is computed from

$$\dot{w} = -C_{EBU}\rho g^{1/2}\left(\frac{\varepsilon}{k}\right) \tag{9}$$

The values of the constants used were those recommended by authors of the papers from which the equations were taken (refs. 3, 5, and 6). These values are as follows:

C_μ	$C_{\varepsilon 1}$	$C_{\varepsilon 2}$	C_{g1}	C_{g2}	C_{EBU}	σ_u, σ_k	σ_ε	Other σ values
0.09	1.43	1.92	2.80	2.00	0.53	1.0	1.3	0.7

As explained in reference 2, C_μ and $C_{\varepsilon 2}$ are modified for axisymmetric flow as follows:

$$C_\mu = 0.09 - 0.04f$$

$$C_{\varepsilon 2} = 1.92 - 0.0667f$$

where

$$f = \left|\frac{Y}{2\Delta U}\left(\frac{\partial u_{cl}}{\partial x} - \left|\frac{\partial u_{cl}}{\partial x}\right|\right)\right|^{0.2}$$

Y radial width of mixing region

ΔU axial direction velocity difference across width of mixing region

---

[1]The ability to calculate reaction rates was not included in the program as received from the contractor; equilibrium chemistry was used there.

Equation (9) for the chemical reaction source term $\dot{w}$ is the same as the one given in reference 3, which was concerned with premixed flow. To use it for diffusion flames, the value of $g^{1/2}$ was taken to be the root mean square of the fluctuations in fuel or oxidant, whichever was smaller. This assumption was necessary, since $\dot{w}$ must vanish if either fuel or oxidant is not present. Unfortunately, the recommended value $C_{EBU} = 0.53$ was not found to give the best fits of calculated results with data. It was necessary to vary its value over a range of at least an order of magnitude. This point is discussed later in the paper.

The program provides for selection of two-dimensional or axisymmetric geometry. Boundaries to the flow may be chosen to be either walls or free boundaries; a symmetry axis can be specified for axisymmetric flow. A choice can be made between H_2 injection or premixed H_2 and air. Chemical reaction can be suppressed, the gases can react at a finite rate, or they can react completely to the extent that they are mixed. A choice can be made between a pressure distribution which varies only in the flow direction and one in which there are nonuniform transverse pressure profiles. Any desired initial profiles of turbulence kinetic energy and its dissipation rate can be specified, or they can be calculated in the program by using a mixing length model. Free-stream levels of k can be specified independently in the two streams. Ignition can be delayed to any point downstream of the initial station.

Although provision is made for the input of initial profiles of seven variables, only profiles of temperature, axial velocity, pressure, and H_2 mass fraction are required; the others (k, ϵ, and v) are optional. Up to 80 profile points may be specified. The initial profile points can be used exactly as specified or interpolation is available to produce any desired number of points up to 80. Interpolation can be linear or by means of a power-law option. Use of the power-law option can concentrate grid points at either boundary or in the center of the grid. Linear interpolation can apply over the whole grid, or in two sections, where the division between sections is at the H_2 jet boundary. Total mass flow of H_2 injected is an input and is used to adjust the initial grid in the H_2 region to insure that the calculated mass flow of H_2 equals the input value. One other option calculates 1/7-power-law velocity variations in the two parts of the flow.

In normal operation the transverse grid covers the mixing region between the H_2 jet and the co-flowing stream and extends a short distance into the free-stream flow. As the mixing region expands, departure from zero of property gradients (either velocity or temperature) near a boundary causes the grid to expand by entraining free-stream fluid, but the total number of grid points is invariant; that is, the grid stretches over a larger region of space to accommodate the additional fluid. If the grid reaches a wall, boundary conditions are reset to fix that boundary at the wall and no more fluid is entrained through that boundary. A corresponding procedure is used if the grid reaches an axis of symmetry. Of course, the calculation can begin with the grid already at the boundaries. One other interesting mode of operation provides for calculating with specified variation of pressure in the principal flow direction, no entrainment of fluid, wall boundary conditions, and with variable (calculated) flow area.

Thermodynamic properties are based on data from the JANAF tables (ref. 8) and are made available in the program by means of the least-squares-adjusted power-law fits described in reference 9. Temperature is obtained by iteration to match the known local value of static enthalpy. Density is calculated from the gas law. Computer storage is 111000_8 and the run time is about 5 minutes on a Control Data Corporation 6600 machine to go 30 jet diameters downstream from the injection point when 61 transverse grid points are used.

It is difficult to assess the accuracy of the finite-difference procedure used to solve the differential equations. A short qualitative discussion of accuracy appears in reference 7 (p. 156), but for practical purposes it was found to be more satisfactory to compare with results obtained from other calculations or with measured data. An important requirement for hydrogen injection studies is that the mass flow of hydrogen integrated over the cross section at any given station be constant; this hydrogen mass flow is found to vary less than 1 percent.

DESCRIPTION OF TEST CASES

The several test cases described here were selected to demonstrate the ability of the program to make useful predictions of the mixing and reaction of hydrogen and oxygen under a variety of conditions. Table I lists the characteristics of those selected.

TABLE I.- CHARACTERISTICS OF TEST CASES

Test case	Supersonic flow	Geometry	Static temperature		Boundary		Reaction	Source
			Inner	Outer	Inner	Outer		
1	Yes	Axisymmetric	251	1495	Axis	Free	Yes	Present report
2	Yes	Axisymmetric	276	1140	Axis	Free	Yes	Reference 10
3	No	Axisymmetric	300	300	Axis	Free	Yes	Reference 11
4	Yes	Axisymmetric	255	219	Axis	Free	No	Reference 12
5	Yes	Plane	254	1270	Wall	Free	Yes	Reference 13
6	Yes	Plane	294	294	Wall	Wall	No	Present report

Test Case 1

For test case 1 (Beach, appendix A), the geometry of the supersonic nozzle and H_2 injector is illustrated in sketch (a):

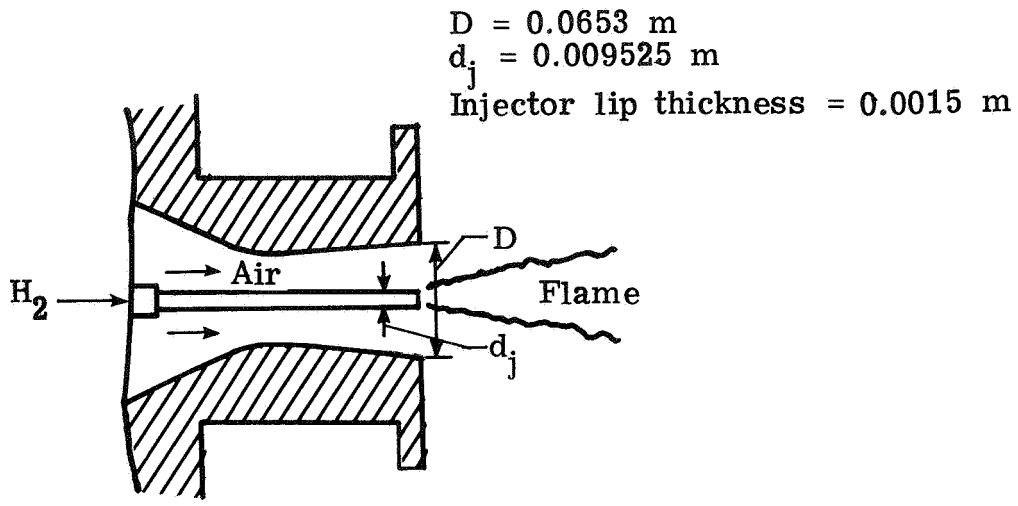

Sketch (a)

The hydrogen was piped from high pressure bottles and was expanded through a supersonic nozzle (not shown) near the end of the injector pipe. A test gas which simulated hot air was obtained by burning H_2 and air, replacing the oxygen, and then expanding through a supersonic nozzle. Data consisted of pitot-pressure profiles and composition profiles. Data at each of the four stations were taken in separate runs. Values of x/d_j for the composition profiles are larger than those for the pitot-pressure profiles because of the geometry of the sampling probes. This and other details are discussed in appendix A. The test conditions for this case are

	Hydrogen jet	Free stream
Mach number, M	2.00	1.90
Temperature, T, K . . .	251	1495
Velocity, u, m/s . . .	2432	1510
Pressure, p, MPa . . .	0.1	0.1
Mass fraction:		
a_{H_2}	1.000	0
a_{O_2}	0	0.241
a_{N_2}	0	0.478
a_{H_2O}	0	0.281

Test Case 2

For test case 2 (Cohen and Guile, ref. 10), the geometry of the supersonic nozzle and H_2 injector is illustrated in sketch (b):

$D = 0.100$ m
$d_j = 0.0200$ m
Injector lip thickness = 0.00054 m

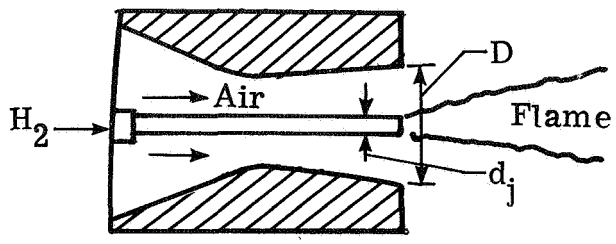

Sketch (b)

The hydrogen was piped from high pressure bottles and was expanded through a supersonic nozzle (not shown) near the end of the injector pipe. A test gas which simulated hot air was obtained by burning H_2 and air, replacing the oxygen, and then expanding through a supersonic nozzle. Data consisted of pitot-pressure profiles, composition profiles, and temperature profiles as given in reference 10. The test conditions for this case are

	Hydrogen jet	Free stream
Mach number, M	1.46	1.86
Temperature, T, K . . .	276	1140
Velocity, u, m/s . . .	1877	1265
Pressure, p, MPa . . .	0.09	0.09
Mass fraction:		
a_{H_2}	1.0	0
a_{O_2}	0	0.260
a_{N_2}	0	0.590
a_{H_2O}	0	0.150

Test Case 3

For test case 3 (Kent and Bilger, ref. 11), the geometry of the air nozzle and H_2 injector is illustrated in sketch (c):

$L = 0.305$ m
$d_j = 0.00762$ m
Injector lip thickness = 0.00020 m

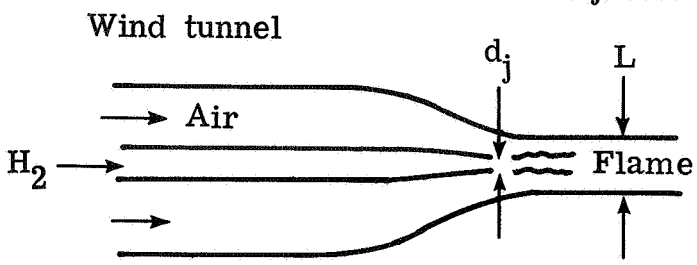

Sketch (c)

The circular H_2 injection nozzle was externally and internally contoured to produce a very thin edge at the exit. Turbulence intensity in the square-sectioned wind tunnel was claimed to be about 0.2 percent. Data consisted of profiles of dynamic pressure, composition, temperature, velocity, and turbulence intensity as given in reference 11. The test conditions for this case are

	Hydrogen jet	Free stream
Mach number, M	0.135	0.043
Temperature, T, K . . .	300	300
Velocity, u, m/s . . .	178	15.1
Pressure, p, MPa . . .	0.1	0.1
Mass fraction:		
a_{H_2}	1.0	0
a_{O_2}	0	0.232
a_{N_2}	0	0.768
a_{H_2O}	0	0

Test Case 4

For test case 4 (Eggers, ref. 12), the geometry of the supersonic nozzle and H_2 injector is illustrated in sketch (d):

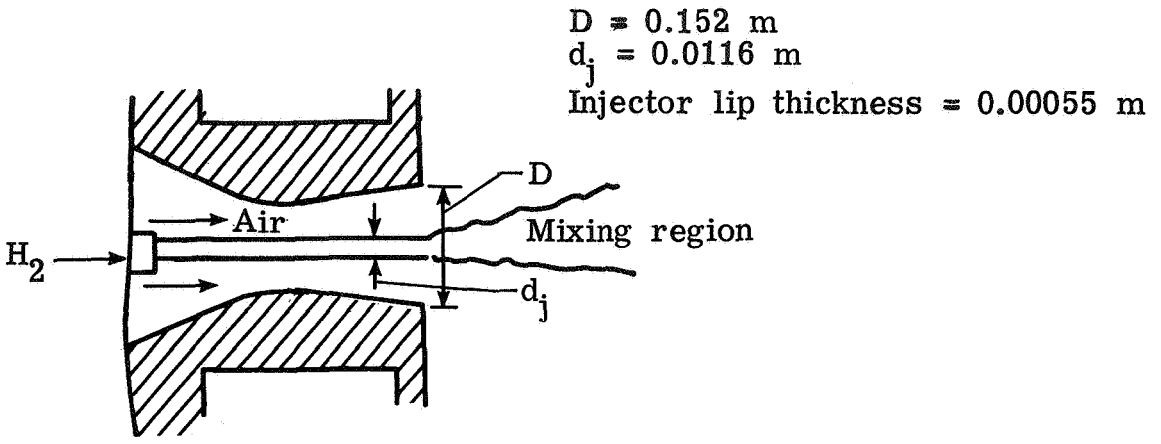

Sketch (d)

The hydrogen was piped from high pressure bottles and was passed through the nozzle at subsonic speed (M = 0.88) into the supersonic airstream (M = 1.32). Data consisted of velocity profiles and composition profiles as given in reference 12. There was no burning because both the hydrogen and the air were cold. The test conditions for this case are

	Hydrogen jet	Free stream
Mach number, M	0.88	1.32
Temperature, T, K . . .	255	219
Velocity, u, m/s . . .	1074	394
Pressure, p, MPa . . .	0.1	0.1
Mass fraction:		
a_{H_2}	1.0	0
a_{O_2}	0	0.232
a_{N_2}	0	0.768
a_{H_2O}	0	0

Test Case 5

For test case 5 (Burrows and Kurkov, ref. 13), the geometry of the two plane mixing layers is illustrated in sketch (e):

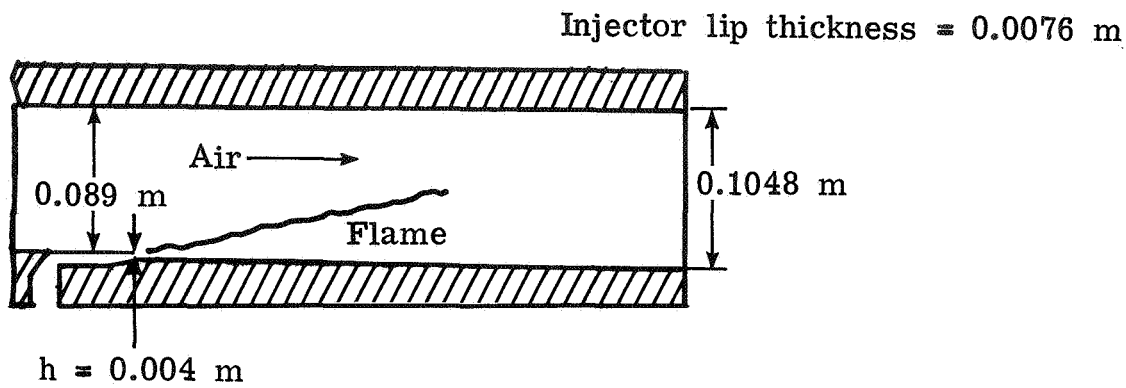

Sketch (e)

Hydrogen was injected at sonic speed through a slot in the lower wall of the test section. A test gas which simulated hot air was obtained by burning H_2 and air, replacing the oxygen, and then expanding through a supersonic nozzle. Data consisted of pitot-pressure profiles, composition profiles, and total temperature profiles as given in reference 13. The test conditions for this case are

	Hydrogen jet	Free stream
Mach number, M	1.00	2.44
Temperature, T, K . . .	254	1270
Velocity, u, m/s . . .	1216	1764
Pressure, p, MPa . . .	0.1	0.1
Mass fraction:		
a_{H_2}	1.000	0
a_{O_2}	0	0.258
a_{N_2}	0	0.486
a_{H_2O}	0	0.256

Test Case 6

For test case 6, the geometry of the supersonic duct is illustrated in sketch (f):

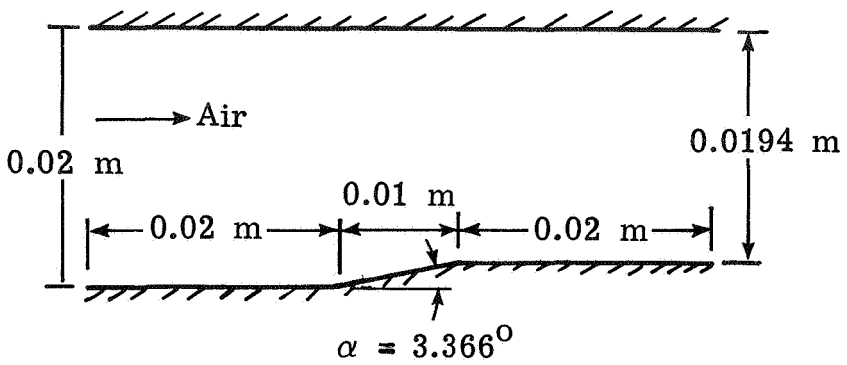

Sketch (f)

Air at Mach 1.5 flows in a two-dimensional duct with walls infinitely distant on two sides. The distance between the other two walls decreases linearly between two given points along the flow direction; everywhere else the walls are parallel. A shock wave with origin at the beginning of the contraction propagates across the flow and reflects from the opposite wall. In similar fashion, a rarefaction with origin at the end of the contraction propagates into the flow. This is not an experimental test case; comparison is made with results obtained from a shock-fitting program (ref. 14). The test conditions for this case are

	Airflow
Mach number, M	1.50
Temperature, T, K . . .	294
Velocity, u, m/s . . .	516
Pressure, p, MPa . . .	0.1
Mass fraction:	
a_{H_2}	0
a_{O_2}	0.232
a_{N_2}	0.768
a_{H_2O}	0

CALCULATED RESULTS

With one exception the experiments described in the test cases have appeared in the literature and are not described here in detail. The data of test case 1, in which hydrogen was injected into a co-flowing, supersonic, axisymmetric, heated airstream, were taken by using the equipment and procedures described in appendix A. The option for computation of transverse pressure profiles was used only for calculating test case 6, which was chosen especially to demonstrate this capability. (There are no experimental data for test case 6.)

The purposes of comparing experimental and calculated results were to validate the use of the program under a variety of conditions and to determine, through experience, any special sensitivities or limitations to its use. The ability of the turbulence model to provide eddy viscosities leading to good prediction of mixing under a wide variety of conditions was of especial interest - as was also the ability to account for the effects of chemical reaction.

Test Case 1

Because test case 1 (Beach, appendix A) to a substantial degree simulates a portion of the reacting flow in a hydrogen-fueled supersonic combustor, and because the measured data are previously unpublished, the analysis is more complete than those for the other cases. Initial profiles at $x/d_j = 0.33$ are given in figure 1 for temperature, pitot pressure, velocity, composition, turbulence kinetic energy, and its rate of dissipation. Static pressure was assumed to be 1 atmosphere throughout the flow field; the composition consisted of hydrogen in the jet and vitiated air outside. The initial static temperature and velocity profiles were based on the known total temperatures in the jet and free stream and on the measured profile of pitot pressure.

The flow calculations began at $x/d_j = 0.33$, the point at which measurements closest to the injector were made. It should be noted that the interior and exterior diameters of the injector were 0.0065 and 0.0095 m, respectively; the lip thickness was 0.0015 m. A small recirculation region probably was present near the lip. If any shock waves were generated by interaction between the jet and the surrounding flow, their effects on the calculated flow properties are not accounted for. Since the jet and free-stream static pressures were carefully matched in the experiments, it is believed that no significant effects caused by such shock waves were present.

Axial variations of pitot pressure and hydrogen mass fraction are shown in figure 2. The reasonable agreement between theory and experiment is a good indication that mixing is calculated correctly. Since mixing is produced by turbulent diffusion in the direction transverse to the axis, and since the magnitude of the diffusion term is proportional to the turbulent viscosity modeled by equation (8), it is important to have a good procedure for determining the initial profiles of k and its dissipation rate ε. Experimental profiles of k and ε were not available; therefore, Prandtl's mixing length theory was used in the manner described in appendix B. Unfortunately, adjustment of the dissipation length parameter ℓ_ε is necessary to achieve good agreement with

the data. To illustrate this point, curves are shown in figure 2 for three values of ℓ_ε.

Since the location of streamlines in a reacting flow can depend strongly on the amount of fuel that reacted, it is also important to examine the radial variation of the integrand in the mass conservation relation:

$$\text{Mass flow} = \int_0^{r_1} \rho u r \, dr \tag{10}$$

In figure 3 experimental[2] and theoretical values of $\rho u r$ at four axial stations are compared. The complete-reaction curve corresponds to an infinitely fast reaction; that is, all fuel and oxygen that mix are completely burned. The quantity C_{EBU} is the constant that appears in equation (9); thus, the curves identified by a value of C_{EBU} were calculated by using equation (9). The no-reaction curve was obtained by using frozen chemical composition. Best agreement is obtained by using $C_{EBU} = 0.10$; the other curves appear on the plots to give the reader a feeling for the range of values to which the calculations are sensitive and to indicate roughly the degree to which reaction is complete. More precisely, for this case ($C_{EBU} = 0.10$), the computed reaction efficiency (defined as the ratio of hydrogen burned to hydrogen macroscopically mixed) is 0.20 at $x/d_j = 6.56$, 0.28 at $x/d_j = 13.8$, 0.30 at $x/d_j = 20.0$, and 0.32 at $x/d_j = 26.2$.

It will become apparent as other test cases are discussed that C_{EBU} is not a constant; its value must be determined by analysis of measured data like that shown in figure 3. Profiles of pitot pressure and composition calculated using $C_{EBU} = 0.10$ are shown in figure 4. No-reaction and complete-reaction curves are shown for comparison. The data points for O_2 are the most sensitive indicator of the degree to which reaction is complete, and these show reasonable agreement with the $C_{EBU} = 0.10$ curves. The data points for H_2O do not agree as well and consistently indicate more water formed than was predicted by the $C_{EBU} = 0.10$ calculation. However, the pitot-pressure data do not reinforce this observation; they indicate less reaction than the $C_{EBU} = 0.10$ calculation. A plausible explanation for this result is that additional reaction takes place in the gas sampling probe. As discussed in reference 15, if this reaction occurs, the gas sample composition is greatly altered, but the pitot pressure is not substantially affected (3 percent to 12 percent maximum).

It should be noted that the eddy breakup model assumes one global reaction ($O_2 + 2H_2 \rightarrow 2H_2O$) and makes the rate proportional to the rate at which large turbulent structures break down into small ones. A model based on a system of chemical kinetic equations would be able to produce H_2O faster in the center of a flame where temperatures and concentrations are high and would produce it slower at the edges. Such an ability might produce calculated curves which agree better with the data.

---

[2]Density and velocity profiles were calculated from the experimental data on pitot pressure and composition.

It should also be remembered that in turbulent flames like the one being examined, unmixedness can play a major role. Since the eddy breakup model is based on the concept of unmixedness, it is likely to be superior in some situations to chemical kinetic models which do not account for unmixedness. It would be desirable to have a model which can account for both chemistry and unmixedness, but such a model is beyond the scope of this report.

Test Case 2

Calculations were made for test case 2 (Cohen and Guile, ref. 10) because the test conditions were similar to those of test case 1. In both experiments hydrogen was axially injected at supersonic speed into a supersonic stream of vitiated air. Geometry was similar and composition profiles were measured downstream in both cases. The most evident differences were in the temperatures of the airstreams (1140 K for this case and 1495 K for test case 1) and in the sizes of the jets (d_j = 0.0200 and 0.009525 m).

The plots in figures 5 to 7 should be compared with those in figures 2 to 4. In both cases the initial value of ℓ_ε was adjusted to give reasonable agreement with the measured data. The distributions of mass flow (figs. 3 and 6) are similar and show that the amount of reaction is small for both cases, although more reaction appears to have occurred in the hotter flow (case 1). For the case 2 finite-rate calculation using $C_{EBU} = 0.05$, the computed reaction efficiency is: 0.14 at $x/d_j = 5.1$, 0.15 at $x/d_j = 8.9$, 0.16 at $x/d_j = 12.7$, and 0.16 at $x/d_j = 17.8$.

The pitot-pressure data in figure 7 and the mass flow distributions in figure 6 agree best with the no-reaction curves, but the H_2O data and the O_2 data indicate that some reaction occurred. The value $C_{EBU} = 0.05$ is used to demonstrate the effect of a small amount of reaction and calculated results obtained with it are not offered as a best fit to the data.

Test Case 3

The experiment for test case 3 (Kent and Bilger, ref. 11) was again axial injection of hydrogen into a co-flowing stream of air. Unlike the two previous cases, the Mach number was low in both streams. Also, the airstream was cold and did not contain the large amount of water present in vitiated air. Great care was taken in the experiment to contour both the hydrogen and the air nozzles so as to produce low initial turbulence; turbulence intensity was claimed to be about 0.2 percent in both the jet and the free stream.

Figure 8 shows the axial variation of several properties for case 3. Except for the momentum flux at the outer edge of the jet $\rho_e u_e^2/(\rho_e u_e^2)_o$, all the properties shown are on the center line. The data extend much farther downstream than in cases 1 and 2 ($x/d_j = 160$ as compared with $x/d_j = 30$). Agreement between theory and experiment is good. The largest discrepancies are in the temperature, and even here the trends are correct.

The mass-flow distributions shown in figure 9 are strikingly different for the no-reaction and the complete-reaction assumptions. Unlike the two previous cases, test case 3 data agree with the assumption of complete reaction rather than that of little or no reaction. The disagreement between theory and data for $r \geqq 0.05$ and $x/d_j \geqq 80$ is thought to be caused by the inability of the $k - \varepsilon$ turbulence model to predict the correct values of turbulent viscosity in the outer region of the flow where velocity gradients are small. Support for this conclusion is contained in the results of an experimental investigation into how large the errors are in the prediction of turbulent viscosity for various flow geometries and in different parts of a flow (ref. 16). The results of the investigation show that for axisymmetric geometry (and plane geometry also), the viscosity is predicted well in the central part of the mixing layer, but not in the low shear regions at the edges. This kind of flaw in the model can be tolerated because the most important viscosity effects occur in the central part of the mixing layer.

The radial profiles shown in figure 10 demonstrate again that the theoretical and experimental results agree well for this case. The agreement is better at $x/d_j = 40$ than at $x/d_j = 120$ and is better for small values of r/d_j than in the outer part of the flow. Best results were obtained with $C_{EBU} = 0.53$. Reaction is nearly complete, as figure 9 also indicated. The computed reaction efficiency is about 0.90 at both $x/d_j = 40$ and at $x/d_j = 120$. The properties of this low-speed diffusion flame are predicted well except in the outer flow region at large distances from the injection point.

Test Case 4

This experiment (test case 4 (Eggers, ref. 12)) is another in which H_2 was injected into a supersonic airstream. There was no reaction, for both gases were cold and there was no ignition. Figure 11 shows the decay of center-line velocity as a function of distance from the injection point and also shows the decay of the H_2 mass fraction along the center line.

The profiles of mass flow are shown in figure 12 for four stations. Both no-reaction and complete-reaction curves are shown, even though case 4 was a nonreacting experiment. This is done to demonstrate a similarity between cases 3 and 4 as compared with cases 1 and 2. The calculated shift of radial position between the no-reaction and complete-reaction curves is much larger for cases 3 and 4. This difference is due to the large density mismatch between the H_2 and air layers for cases 3 and 4.

Consider the effect of density and velocity profiles on the ρur plots. If ρu values were constant across the mixing layer, the plot would be a straight line. In the initial stages, before much mixing occurs, the curve consists essentially of two straight lines which correspond to the two free-stream conditions. The following tables are helpful for comparing the ρur plots of the four cases:

Case	H_2 layer		
	ρ	u	ρu
1	0.098	2432	238
2	.080	1877	150
3	.082	178	15
4	.096	1074	103

Case	Air layer		
	ρ	u	ρu
1	0.203	1510	307
2	.257	1265	324
3	1.17	15	18
4	1.61	394	634

Case	Ratios (Air/H_2)	
	ρu	ρ
1	1.29	2.4
2	2.16	3.2
3	1.21	14.3
4	6.16	16.7

The air/H_2 ratios of ρu for cases 1 and 3 are both near unity. Thus, the slopes of the two parts of the no-reaction curves should be nearly the same. The ratios of the slopes are about 2 for case 2 and about 6 for case 4. Crude confirmation of these relationships can be had by examining figures 3, 6, 9, and 12.

As was remarked earlier, the density ratios are larger for cases 3 and 4 than for cases 1 and 2; the outer layers are cold air instead of hot air. When reaction occurs, density drops in that part of the cold air near the flame front and the streamlines expand to satisfy mass conservation. The effect would be the same if the H_2 stream and air stream were interchanged; the radial shifts would still be away from the center line and they would be larger for larger density ratios.

It is apparent that ρur plots can be used to determine the amount of reaction present, even with quite crude values of measured composition. This is a very useful capability, since it is often difficult to be sure that the measured sample profiles are representative of the flow being sampled.

The center-line data for case 4 have been compared previously (ref. 17) with calculations made by using the same $k - \varepsilon$ turbulence model used here. The agreement was better than that in figure 11, but profiles were not reported. In the present calculation, close attention was given to obtaining good agreement with the profiles, as shown in figures 12 and 13, but at the cost of somewhat poorer agreement with center-line data. The agreement is better for velocity profiles than for the H_2 mass fraction profiles, but for both, the results are acceptable, and the trends indicated are correct.

Test Case 5

Test case 5 (Burrows and Kurkov, ref. 13) is the only mixing experiment considered in which H_2 was not injected along the center line of an axisymmetric airstream; injection in this case was from a slot in a step on the wall of a rectangular duct. As shown in figure 14, agreement between theory and experiment is good when a nearly complete reaction is assumed. In fact, the only place in the figure where the finite rate and complete reaction curves differ appreciably is near the peak of the curve for mole fraction of water.

The agreement is considerably better than that obtained by the authors of reference 13. Their calculated profile shapes, including the peak of the water profile, matched those of the data well, but were misplaced in the cross-stream direction. They discussed the discrepancy themselves and suggested two possible explanations: (1) that the use of equilibrium, rather than finite-rate chemistry, was responsible for the difference; and (2) that effective viscosity was higher in the flame region than their model predicted. They obtained excellent agreement between theory and experiment when they examined data obtained in a nonreacting experiment similar to the reacting one.

Test Case 6

Test case 6 was chosen to illustrate the program's capability for calculating transverse pressure profiles. No suitable measured data were available, but a good test case was obtained by analyzing the chosen flow field by using the shock fitting program described in reference 14.

Air at room temperature and Mach number 1.5 flows between two plates. All property profiles are initially uniform. Between the two given points, the distance between the plates decreases linearly; elsewhere, the distance between them is a constant. A shock wave, with origin at the first point, moves into the flow and is reflected from the opposite wall. In similar fashion, a rarefaction moves into the flow from the second point.

The solid lines in figure 15 show the shock fitting results and the other lines show the results obtained with the parabolic marching program. Obviously, steep pressure gradients, like the shock waves in figure 15(a), are poorly represented. However, the general shape and magnitude of the pressure profiles are obtained, and both the shock wave and the rarefaction region are easily identified.

It is interesting to note how the diffuse shock fronts calculated by the program cause premature pressure changes at the walls. (See fig. 15(b).) No premature pressure change is calculated on the lower wall at $y = 0.01$ m or at $y = 0.03$ m because these changes were initiated by sudden changes of slope in the lower wall. In the program, flow area is caused to match duct area by adjusting the average pressure in a one-dimensional approximate treatment. This is a better approximation in subsonic flow than in supersonic flow, because the finite time required for pressure changes to propagate is ignored in the one-dimensional treatment. For an example of this effect, see figure 15(b), in which pressure at a wall should be constant except when a shock wave or a rarefaction passes. The overall raising of the pressure which can be seen in the calculated results is caused by accounting in the one-dimensional treatment for boundary-layer growth at the walls. Because of the tendency of shock and expansion waves to be diffused by mixing and reaction, detailed calculation of their propagation in supersonic combustors may not be warranted for many applications. The extent to which transverse pressure gradients can be accounted for in the present program should be useful in such cases.

CONCLUDING REMARKS

The two-dimensional computer program described here is a useful tool for analysis of a variety of turbulent flows - namely, mixing between parallel streams, plane or axisymmetric, subsonic or supersonic, ducted or nonducted, reacting or nonreacting. The test cases demonstrate that this program can be used to calculate properties of such flows with reasonable accuracy. They also demonstrate that good modeling of both turbulence and reaction effects is necessary for calculation of flow properties in turbulent flames. The empirical constants in the turbulence model were the same for all calculations (assumed universality of the model), but the initial profiles of turbulence kinetic energy k and dissipation rate of turbulence kinetic energy ε were found to strongly influence the results. The eddy breakup model (modified) for calculating the rate of chemical reaction produced composition profiles which in most cases closely resembled the measured profiles, but was able to do so only by adjusting an empirical constant to cause calculated profiles of mass flow distribution to match those measured. Adjustment of this constant controlled the amount of heat released by chemical reaction and thereby determined the spatial location of streamlines in the flow through the change in gas density profiles.

The two-equation turbulence model appears to be generally adequate for modeling turbulent viscosity in axisymmetric and two-dimensional plane flows, except in regions of low shear. Plots of mass flow distribution are very useful for deciding how much reaction occurred in a given experiment. The eddy breakup model (modified), which is valid only if a flame is diffusion controlled, gave reasonable results for the cases reported, but should be replaced by a chemical kinetic model, if one can be developed, which adequately accounts for the effects of turbulence.

Langley Research Center
National Aeronautics and Space Administration
Hampton, VA 23665
February 17, 1978

APPENDIX A

DATA FOR TEST CASE 1

In order to provide additional data for the evaluation of analytical models under development, a mixing-reacting experiment was conducted at the Langley combustion test stand. The experiment consisted of the injection of a supersonic jet of hydrogen coaxially into a high-temperature, vitiated airstream.

Apparatus and Procedure

The test gas for the experiment was generated by burning hydrogen in air and replenishing the volumetric oxygen content. The heater which accomplishes this is described in detail in reference 18; it is capable of producing stagnation temperatures to 2800 K and stagnation pressures to 3.1 MPa. Extensive facility calibration has indicated virtually 100 percent combustion efficiency for the heater, and the primary test gas constituents are therefore oxygen, nitrogen, and water vapor.

The test gas nozzle, which is constructed of stainless steel, is cooled by approximately 6 kg/sec of water. The exit diameter is 6.57 cm, and the exit Mach number is approximately 1.9. A stagnation pressure of 0.067 MPa was required to achieve the desired 1-atmosphere static-pressure condition at the nozzle exit. Stagnation temperature was nominally 2250 K in order to simulate flight enthalpy environments in the Mach 7 regime. The resulting static temperature and test-gas flow rate were approximately 1500 K and 0.980 kg/sec. Nominal test gas constituents were oxygen (20%), water vapor (38%), and nitrogen (42%) by volume.

The hydrogen injector at the nozzle center line is a 0.95-cm-diameter stainless-steel tube with a nozzle insert that produces a 5° exit half-angle. The exit Mach number is nominally 2, and the lip thickness approximately 1.5 mm. In these tests cooling was provided by the injectant which originated from a supply at ambient temperature. Hydrogen stagnation pressure was adjusted to provide a matched-pressure condition at the injector and test gas nozzle exits. Estimated temperature rise for the hydrogen passing through the injector was 150 K; this gave a hydrogen stagnation temperature of 450 K, and a hydrogen mass flow rate of 0.0084 kg/sec.

Primary in-stream measurements for the experiment were pitot pressure and composition profiles. Details of the pitot probe design are given in reference 19. Briefly, the probe tip is a 20° half-angle cone with a 0.79-mm orifice. The maximum diameter at the base of the probe tip is 0.92 cm. A continuous traverse of the flow was made at a rate of 0.5 cm/sec. Pressure surveys were taken at x/d_j locations of 0.33, 6.56, 13.8, 20, and 26.2; the data appear in figures 1 to 4 and in table A1. Gas samples were taken with a wedge gas sampling probe discussed in reference 20. It has a 20° included angle with the sampling surface mounted at 2° to the flow; ports 0.5 mm in diameter are drilled 2.4 mm apart. The wedge leading edge has a 0.38-mm radius to reduce stagnation-point heating. Gas samples were acquired at x/d_j locations of

TABLE A1.- PITOT-PRESSURE SURVEYS

(a) $x/d_j = 0.33$; $p_{ref} = 0.676$ MPa

r/d_j	$p_{t,2}/p_{ref}$
3.085	0.633
2.925	.693
2.495	.703
2.135	.767
1.785	.728
1.505	.733
1.385	.693
1.145	.678
.675	.673
.597	.559
.518	.474
.439	.294
.360	.713
.241	.713
.202	.882
.0045	.862
-.153	.857
-.232	.777
-.351	.658
-.430	.284
-.548	.479
-.745	.658
-1.065	.678
-1.335	.673
-1.655	.688
-1.925	.727
-2.205	.728
-2.525	.708
-2.755	.693
-3.035	.693

(b) $x/d_j = 6.56$; $p_{ref} = 0.680$ MPa

r/d_j	$p_{t,2}/p_{ref}$
3.02	0.406
2.74	.713
2.55	.752
2.03	.718
1.68	.703
1.32	.693
1.08	.688
.732	.663
.613	.530
.495	.377
.297	.565
.1395	.802
-.058	.787
-.137	.743
-.255	.565
-.492	.396
-.610	.490
-.729	.634
-.768	.668
-1.04	.668
-1.56	.688
-1.91	.703
-2.27	.713
-2.54	.728
-2.82	.752
-3.05	.723

(c) $x/d_j = 13.8$; $p_{ref} = 0.703$ MPa

r/d_j	$p_{t,2}/p_{ref}$
3.07	0.381
2.88	.552
2.57	.683
3.42	.712
2.23	.712
2.0	.697
1.81	.697
1.38	.688
1.12	.688
.88	.678
.81	.639
.731	.527
.539	.391
.27	.518
.04	.649
-.191	.532
-.537	.381
-.806	.586
-.921	.693
-1.113	.702
-1.42	.697
-1.65	.683
-1.92	.678
-2.19	.688
-2.53	.688
-2.80	.678
-3.0	.620

(d) $x/d_j = 20.0$; $p_{ref} = 0.680$ MPa

r/d_j	$p_{t,2}/p_{ref}$
2.99	0.377
2.72	.496
2.32	.609
2.08	.674
1.77	.689
1.37	.703
1.29	.708
1.058	.679
.742	.451
.584	.416
.308	.471
.0711	.520
-.008	.525
-.205	.481
-.521	.416
-.718	.456
-.955	.599
-1.15	.689
-1.23	.713
-1.59	.703
-1.86	.689
-2.49	.664
-3.09	.486

(e) $x/d_j = 26.2$; $p_{ref} = 0.678$ MPa

r/d_j	$p_{t,2}/p_{ref}$
2.84	0.398
2.33	.537
2.05	.616
1.70	.651
1.38	.656
1.19	.621
.988	.541
.712	.422
.554	.412
.317	.422
-.002	.452
-.354	.432
-.551	.412
-.788	.412
-1.06	.467
-1.38	.641
-1.70	.670
-2.01	.666
-2.37	.651
-2.68	.601
-3.31	.407

8.26, 15.5, 21.7, and 27.9, and the results are shown in figures 1 to 4 and in table A2. The difference in axial location between the pitot and gas sample surveys is caused by the fact that the wedge-probe and pitot-probe leading edges were at the same location, but the sampling ports are 1.7 cm behind the wedge leading edge.

Gas samples were collected in 75-cm^3 cylinders (with valves at each end) by evacuating them, purging with the sample gases during a run, and finally filling them to an appropriate pressure level with the sample gases. Total sampling time for a set of nine samples was 8 seconds. Analysis was by gas chromatograph, and only dry samples of nitrogen, hydrogen, oxygen, and helium were examined;[3] helium was used to trace the replenishment oxygen in order to differentiate it from the oxygen in air. Water concentrations were deduced from the dry samples by a data-reduction technique described in reference 19. A quantitative indication of the validity of this approach is given by comparison of the reduced free-stream levels of nitrogen, oxygen, and water vapor as compared with the bulk values in the heater. (See fig. 4.)

It should be noted that facility and instrumentation limitations allowed only one profile to be obtained in any given burner firing. The nine surveys (five pitot, four composition) were therefore obtained in nine different runs, and some differences in test gas and hydrogen flow rates were inevitable. However, these differences were slight, with maximum deviations of 1.1 percent, 3.8 percent, and 2.2 percent from previously mentioned heater stagnation pressure, stagnation temperature, and hydrogen fuel flow rate, respectively. The stagnation temperatures were not measured directly but were computed from heater performance data and the measured flow rates of hydrogen, oxygen, and air to the heater.

Data Integrity

A traditional indicator of data integrity for mixing flow fields has been the comparison of mass flows calculated from measured composition profiles with flow rates measured during the experiment. For these free-jet data, the only meaningful comparison is for injected hydrogen. Integrations utilizing the composition, pitot pressure, and an assumed uniform static pressure of 1 atmosphere were made at the four sample locations. It was assumed that the closest pitot profile to each wedge location was valid at the wedge location. Errors resulting from the integration process ranged from 25 to 33 percent. These are large errors, although magnitudes of 20 percent are typical for this type of flow field. There are several potential sources for the discrepancies.

Data accuracy of pitot pressure measurements in flows in local thermodynamic equilibrium is typically very reliable, and results from the dry samples analyzed by the chromatograph are good to within ±1 percent. However, it is possible that the probes complete an on-going reaction, and that the constituents reaching the sample bottle are not those which were present ahead of the probe. If account is taken for this effect by the unreacting of part of the

---

[3]The water was removed before analysis because condensation in the sampling tubes would invalidate any attempt to include it in the analysis.

TABLE A2.- SPECIE MASS FRACTIONS

(a) $x/d_j = 8.26$

r/d_j	Mass fraction for -				
	H_2O	H_2	O_2	N_2	Ar
-0.275	0.232	0.574	0	0.190	0.003
.025	.141	.742	0	.115	.002
.225	.195	.642	0	.160	.003
.475	.466	.094	.025	.408	.007
.725	.300	0	.229	.462	.008
.975	.267	0	.259	.465	.008
1.225	.257	0	.268	.466	.008
1.475	.247	0	.276	.468	.008
1.725	.244	0	.278	.469	.008

(b) $x/d_j = 15.5$

r/d_j	Mass fraction for -				
	H_2O	H_2	O_2	N_2	Ar
-0.283	0.315	0.423	0	0.257	0.005
-.033	.215	.604	0	.177	.004
.227	.263	.517	0	.216	.004
.477	.450	.163	.004	.376	.007
.727	.393	.008	.137	.453	.008
.977	.332	0	.198	.461	.008
1.227	.322	0	.207	.463	.008
1.477	.274	0	.250	.467	.008
1.727	.270	0	.253	.468	.008

(c) $x/d_j = 21.7$

r/d_j	Mass fraction for -				
	H_2O	H_2	O_2	N_2	Ar
-0.265	0.353	0.353	0	0.288	0.005
-.015	.312	.428	0	.255	.005
.235	.341	.374	0	.280	.005
.485	.431	.205	0	.357	.006
.735	.440	.037	.078	.437	.008
.985	.362	.002	.169	.459	.008
1.23	.311	0	.217	.463	.008
1.49	.274	0	.250	.466	.008
1.735	.269	0	.255	.468	.008

(d) $x/d_j = 27.9$

r/d_j	Mass fraction for -				
	H_2O	H_2	O_2	N_2	Ar
-0.267	0.403	0.262	0	0.329	0.006
-.017	.369	.323	0	.303	.005
.233	.394	.275	0	.324	.006
.483	.429	.162	.024	.377	.007
.733	.445	.527	.065	.429	.008
.983	.380	.006	.149	.456	.008
1.233	.347	.001	.183	.461	.008
1.483	.301	0	.224	.466	.008
1.733	.263	0	.260	.468	.008

fuel, a 5-percent increase in hydrogen mass flow results from 50-percent local unreactedness and 13 percent from 90-percent unreactedness.

Another possible error source is probe alignment. If the assumption is made that the wedge probe was on a chord displaced 0.16 cm off the diameter, increases in computed hydrogen mass flows range from 15 percent at $x/d_j = 8.26$ to 7 percent at $x/d_j = 27.9$. It is difficult to assess the errors produced by sampling pitot pressures and composition at slightly different locations, but they are believed to be small.

The assumption of uniform static-pressure profiles is obviously not correct even though the pressures of hydrogen and test gas are initially matched. The injector has a conical nozzle, and the lip thickness of the injector is large enough to cause aerodynamic disturbances. Nevertheless, if a uniform increase of 10 to 15 percent is made in the static pressure, the computed mass flow increases only 2 to 3 percent.

Other possible sources of error include the heat loss in the heater and nozzle (change in mass flow is 2 percent maximum), and the fact that oxygen and helium may not diffuse together (less than 2 percent error).

Unfortunately, hardware problems eliminated the possibility of examining and correcting these potential error sources. In spite of this, the data are believed to be representative and meaningful and are appropriate for the evaluations being made in this report.

APPENDIX B

PROCEDURE FOR DETERMINATION OF INITIAL PROFILES OF k AND ε

Turbulent viscosity is modeled by using equation (8) in combination with equations (4) and (5). The initial profiles of k and ε used to begin calculations with these equations have a marked influence on the amount of mixing calculated. Since measured profiles of k and ε are seldom available, the following procedure has been devised for use in their absence.

First, an estimate is made of background levels of turbulence in each stream; these are put in as constant values of k to which shear-generated peaks are added. The shear-generated peaks at the initial station are calculated by using a mixing-length equation; the result of summing the two contributions is

$$k = \left(\frac{\ell_\varepsilon}{0.3}\frac{\partial u}{\partial y}\right)^2 + k_{background} \tag{B1}$$

where ℓ_ε is the dissipation length scale,

$$\ell_\varepsilon \equiv \frac{C_\mu k^{3/2}}{\varepsilon} \tag{B2}$$

The length scale ℓ_ε is chosen equal to 10 times an appropriate physical dimension such as the thickness of the splitter plate in a two-dimensional free shear layer experiment; it is then adjusted to obtain best agreement with observed quantities downstream. Given the k profile from equation (B1), the ε profile is calculated from equation (B2).

The viscosity μ, calculated from equation (8), is a turbulent viscosity. In the program the laminar viscosity is computed and is added to μ, so that the viscosity used in all transport equations is the sum of the laminar and turbulent viscosities. Usually, the laminar viscosity makes a negligible contribution to the total.

Equation (B2) is a definition. Equation (B1) is derived from Prandtl's mixing length equation as follows:

$$\mu = \rho \ell_m^2 \left(\frac{\partial u}{\partial y}\right) \tag{B3}$$

This equation is appropriate for flows in which the production term for k is equal to the dissipation term, and experiments have shown that for such flows (ref. 21),

$$\tau \equiv \mu\left(\frac{\partial u}{\partial y}\right) = 0.3\rho k \tag{B4}$$

APPENDIX B

By combining equations (8) and (B2),

$$\mu = \rho k^{1/2} \ell_\varepsilon \tag{B5}$$

From equations (B3) to (B5),

$$\ell_m{}^2 = \frac{\ell_\varepsilon{}^2}{0.3} \tag{B6}$$

$$k = \left(\frac{\ell_\varepsilon}{0.3} \frac{\partial u}{\partial y}\right)^2 \tag{B7}$$

Equations (B1) and (B2) are adequate to define initial profiles of k and ε based on the Prandtl mixing length concept; the only information needed is a characteristic dissipation length ℓ_ε and a velocity profile. Experience with this approach has been good, provided some experimental knowledge is available about the downstream flow so that the value of ℓ_ε can be adjusted. A more satisfactory procedure would be to find ℓ_ε by referring to a correlation plot in terms of known physical quantities so that flow-field predictions could be made reliably without reference to measured downstream properties. Unfortunately, no such relation has been found.

REFERENCES

1. Waltrup, Paul J.; Anderson, Griffin Y.; and Stull, Frank D.: Supersonic Combustion Ramjet (Scramjet) Engine Development in the United States. 3rd International Symposium on Air Breathing Engines - Proceedings (Munich), DGLR-Fachbuch Nr. 6, Mar. 1976, pp. 835-861.

2. Launder, B. E.; and Spalding, D. B.: The Numerical Computation of Turbulent Flows. Comput. Methods Appl. Mech. & Eng., vol. 3, no. 2, Mar. 1974, pp. 269-289.

3. Lilley, David G.: Turbulent Swirling Flame Prediction. AIAA J., vol. 12, no. 2, Feb. 1974, pp. 219-223.

4. Free Turbulent Shear Flows. Volume I - Conference Proceedings. NASA SP-321, 1973.

5. Spalding, D. B.; Launder, B. E.; Morse, A. P.; and Maples, G.: Combustion of Hydrogen-Air Jets in Local Chemical Equilibrium (A Guide to the CHARNAL Computer Program). NASA CR-2407, 1974.

6. Elghobashi, S.; and Spalding, D. B.: Equilibrium Chemical Reaction of Supersonic Hydrogen-Air Jets (The ALMA Computer Program). NASA CR-2725, 1977.

7. Patankar, S. V.; and Spalding, D. B.: Heat and Mass Transfer in Boundary Layers. Second ed. Int. Textbook Co., Ltd. (London), c.1970.

8. JANAF Themochemical Tables - Second Edition. NSRDS-NBS 37, U.S. Dep. Commer., June 1971.

9. McBride, Bonnie J.; Heimel, Sheldon; Ehlers, Janet G.; and Gordon, Sanford: Thermodynamic Properties to 6000° K for 210 Substances Involving the First 18 Elements. NASA SP-3001, 1963.

10. Cohen, Leonard S.; and Guile, Roy N.: Investigation of the Mixing and Combustion of Turbulent, Compressible Free Jets. NASA CR-1473, 1969.

11. Kent, J. H.; and Bilger, R. W.: Measurements in Turbulent Jet Diffusion Flames. TN F-41, Dept. Mech. Eng., Univ. Sydney (Australia), Oct. 1972.

12. Eggers, James M.: Turbulent Mixing of Coaxial Compressible Hydrogen-Air Jets. NASA TN D-6487, 1971.

13. Burrows, Marshall C.; and Kurkov, Anatole P.: Analytical and Experimental Study of Supersonic Combustion of Hydrogen in a Vitiated Airstream. NASA TM X-2828, 1973.

14. Salas, Manuel D.: Shock Fitting Method for Complicated Two-Dimensional Supersonic Flows. AIAA J., vol. 14, no. 5, May 1976, pp. 583-588.

15. Eggers, James M.; Reagon, Patricia G.; and Gooderum, Paul B.: Combustion of Hydrogen in a Two-Dimensional Duct With Stop Fuel Injectors. NASA TP-1159, 1978.

16. Rodi, W.: A Note on the Empirical Constant in the Kolmogorov-Prandtl Eddy-Viscosity Expression. Trans. ASME, Ser. I: J. Fluids Eng., vol. 97, no. 1, Mar. 1975, pp. 386-389.

17. Launder, B. E.; Morse, A.; Rodi, W.; and Spalding, D. B.: Prediction of Free Shear Flows - A Comparison of the Performance of Six Turbulence Models. Free Turbulent Shear Flows. Volume I - Conference Proceedings, NASA SP-321, 1973, pp. 361-426.

18. Russin, William Roger: Performance of a Hydrogen Burner To Simulate Air Entering Scramjet Combustors. NASA TN D-7567, 1974.

19. Eggers, James M.: Composition Surveys of Test Gas Produced by a Hydrogen-Oxygen-Air Burner. NASA TM X-71964, 1974.

20. Beach, H. Lee, Jr.: Evaluation of a Wedge Gas-Sampling Probe. AIAA J., vol. 12, no. 9, Sept. 1974, pp. 1284-1286.

21. Harsha, P. T.; and Lee, S. C.: Correlation Between Turbulent Shear Stress and Turbulent Kinetic Energy. AIAA J., vol. 8, no. 8, Aug. 1970, pp. 1508-1510.

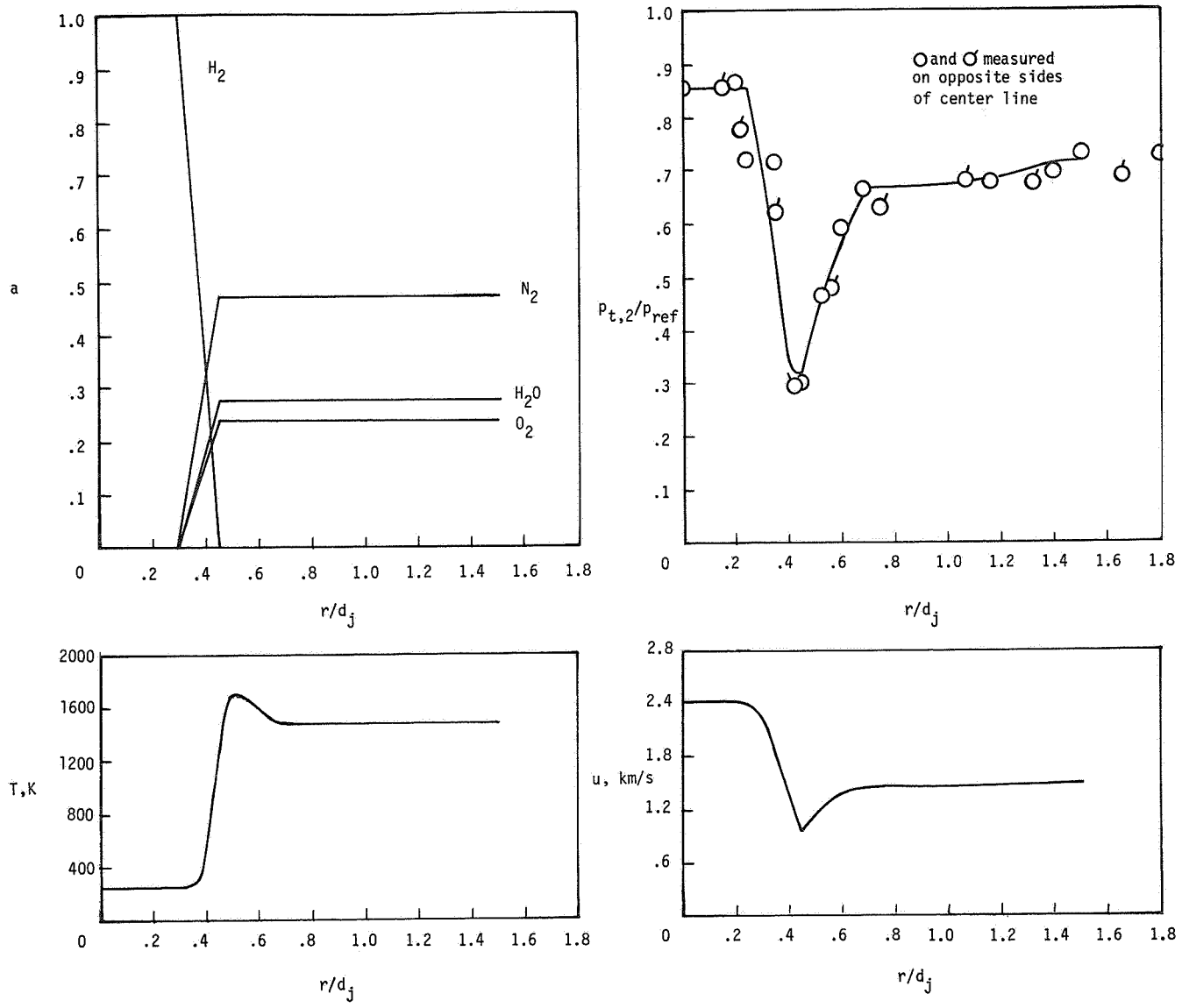

(a) Mass fraction, temperature, pitot pressure, and velocity.

Figure 1.- Initial property profiles for case 1. $x/d_j = 0.33$. (H_2 in jet; vitiated air outside.)

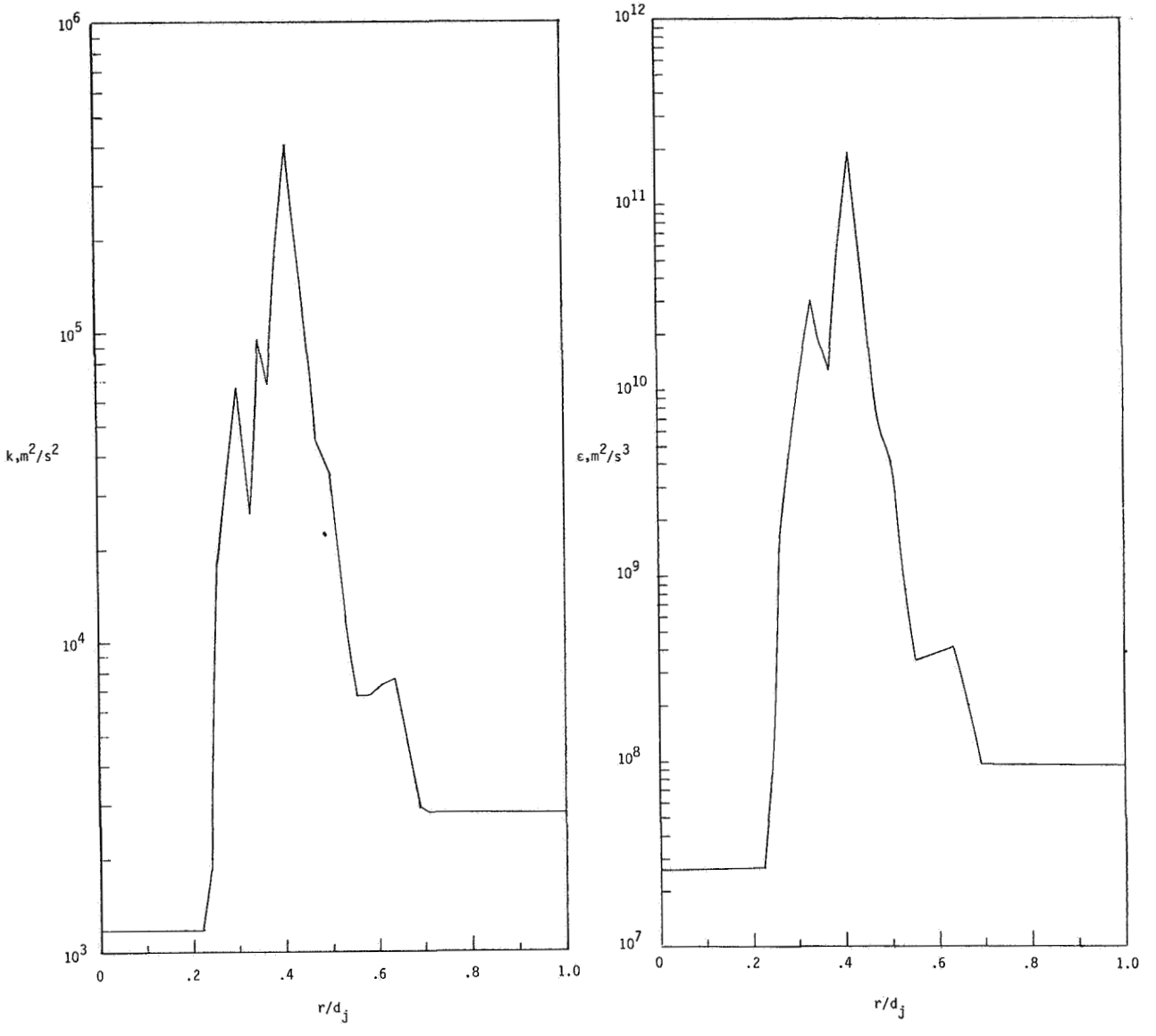

(b) Turbulent kinetic energy and its dissipation rate.

Figure 1.- Concluded.

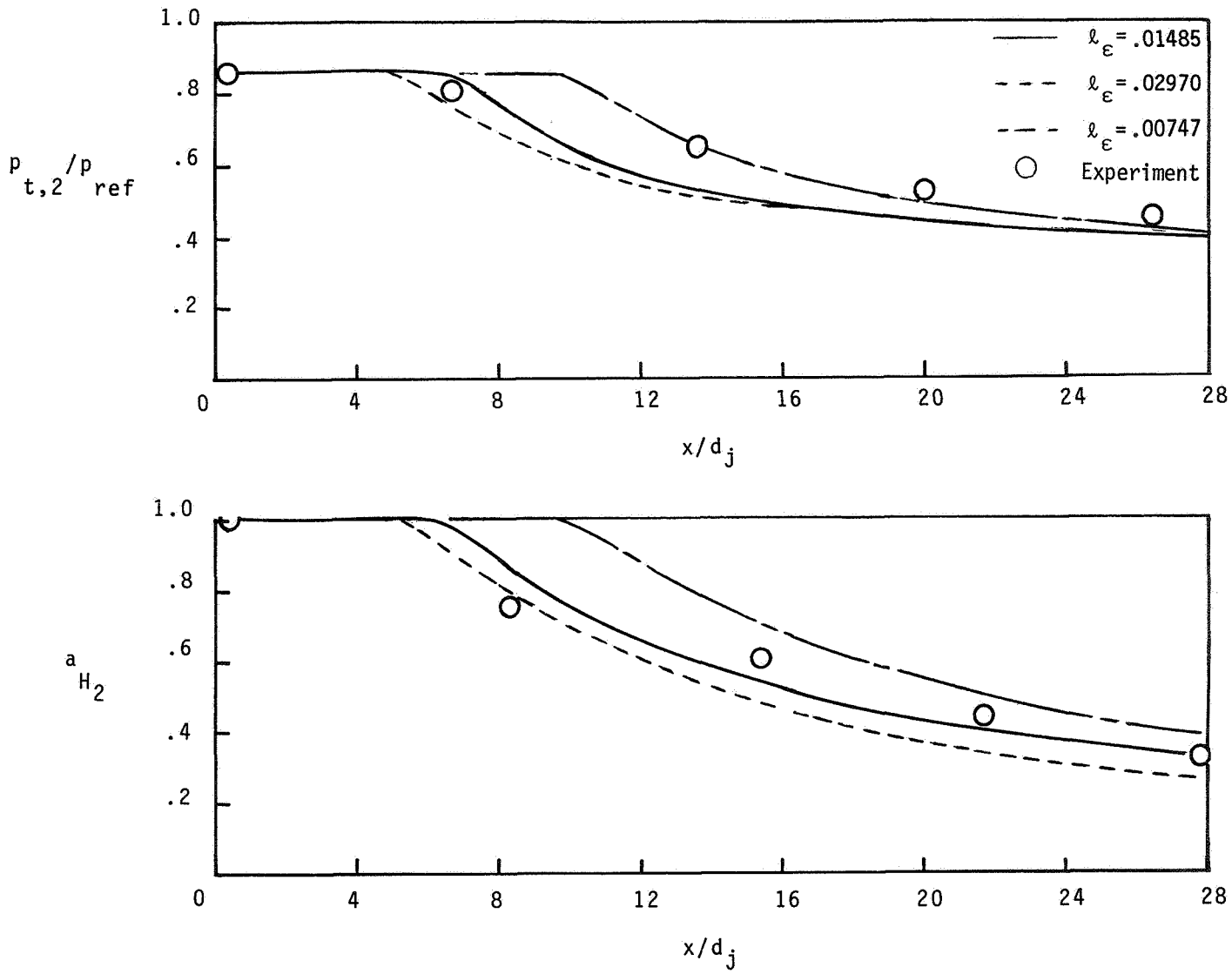

Figure 2.- Axial variation of pitot pressure and hydrogen mass fraction on the center line for case 1. $C_{EBU} = 0.10$. (H_2 in jet; vitiated air outside.)

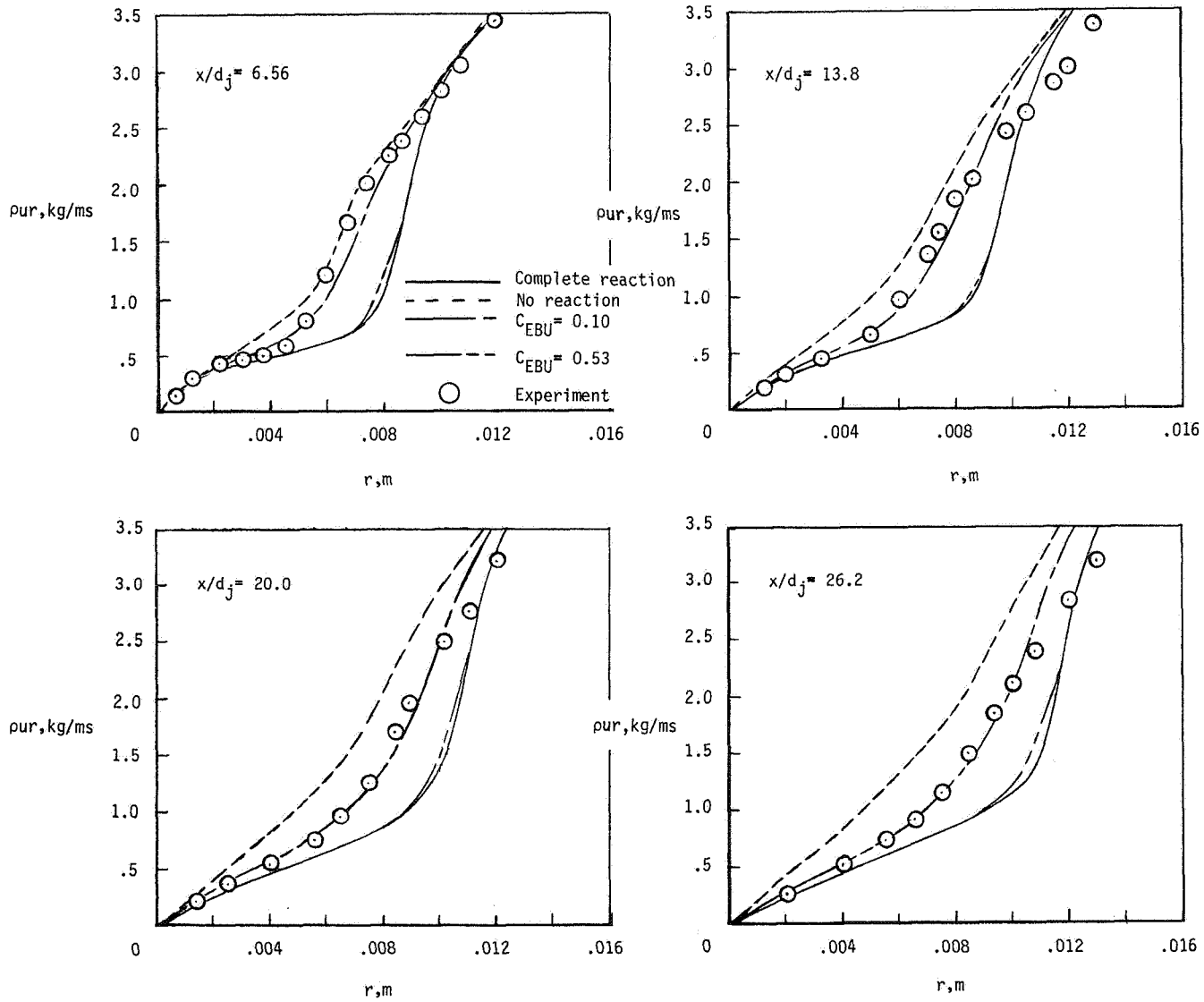

Figure 3.- Distribution of mass flow for case 1. (H_2 in jet; vitiated air outside.)

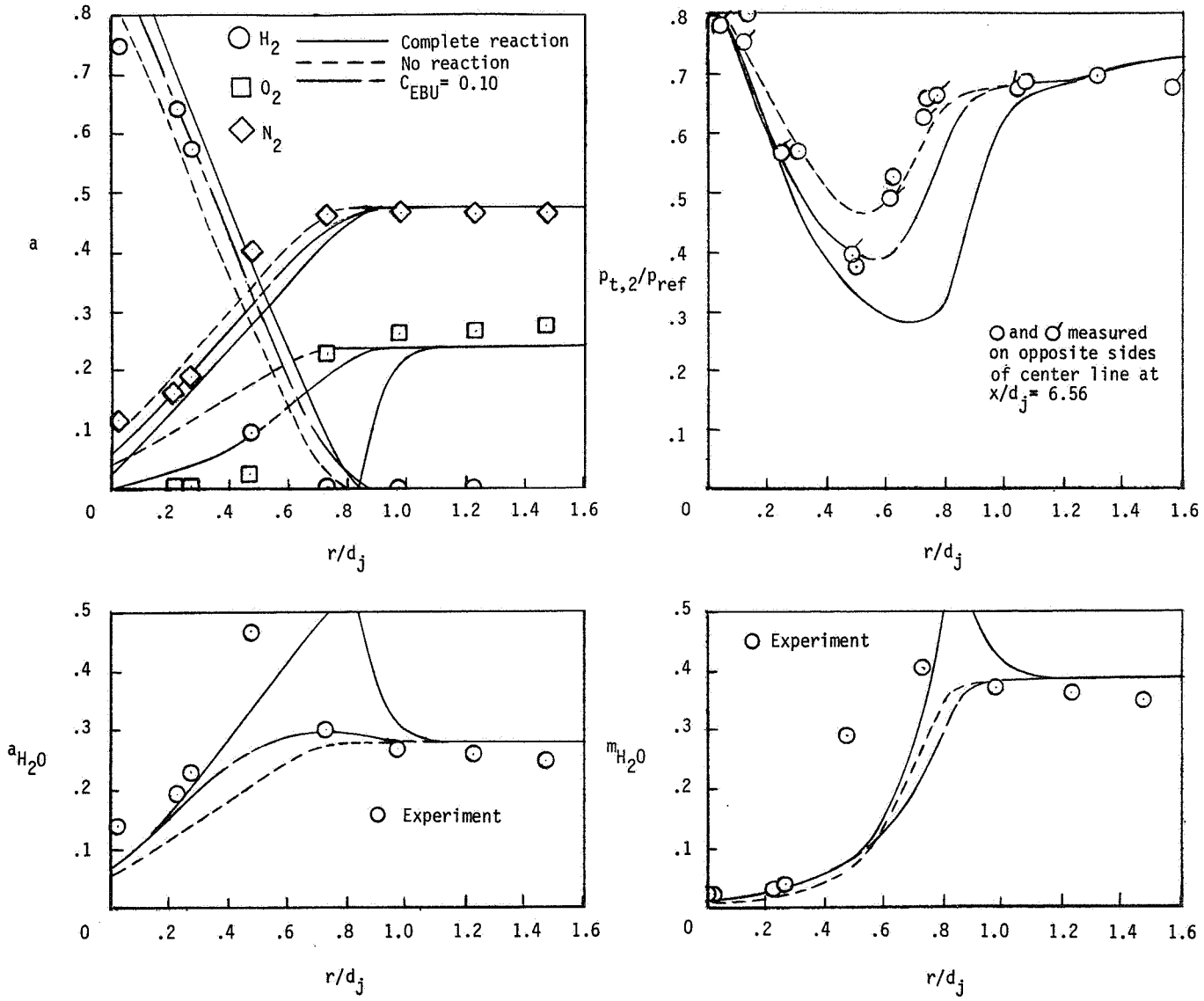

(a) $x/d_j = 8.26$ except for $p_{t,2}/p_{ref}$.

Figure 4.- Profiles of composition and pitot pressure for case 1. (H_2 in jet; vitiated air outside.)

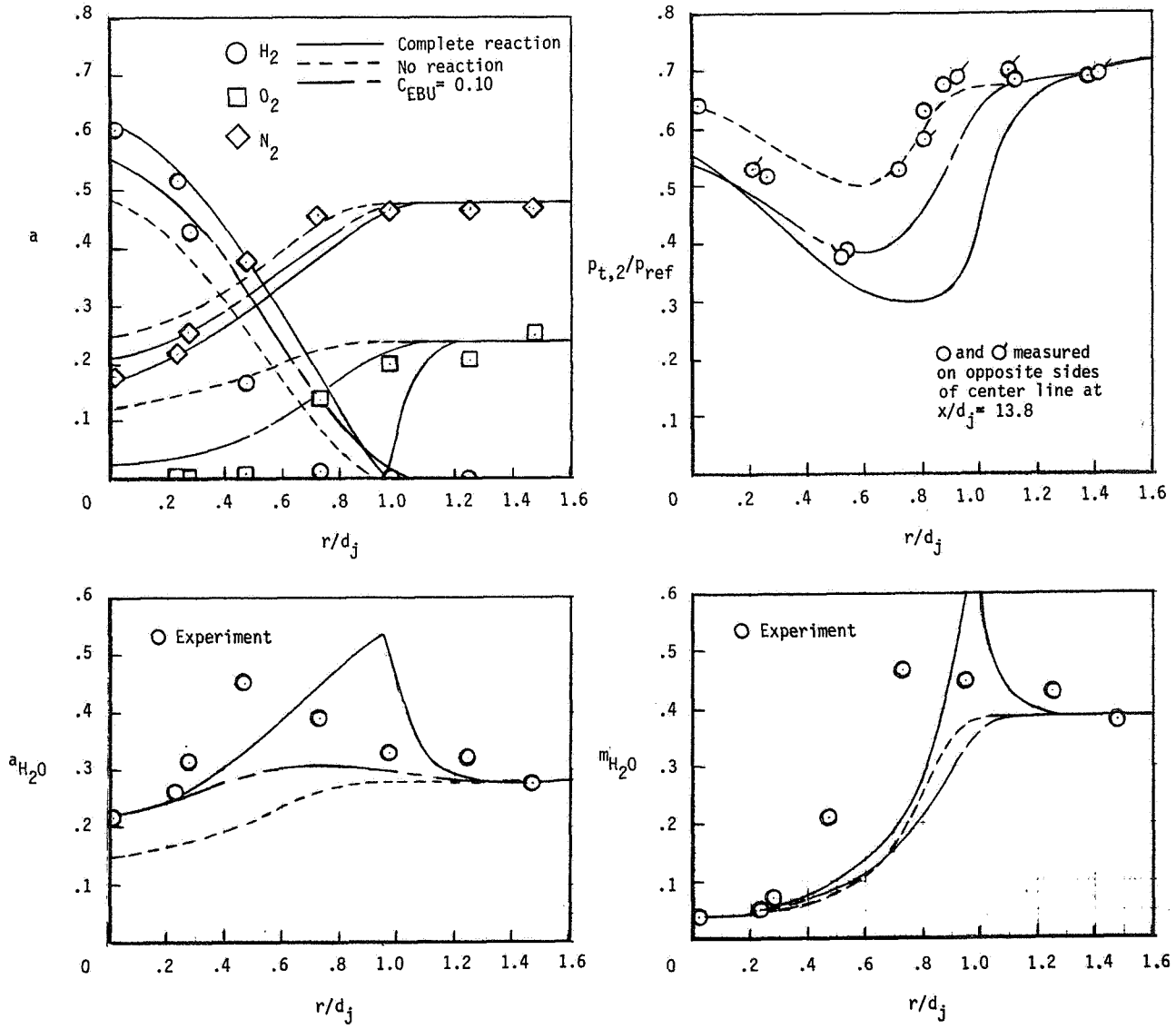

(b) $x/d_j = 15.5$ except for $p_{t,2}/p_{ref}$.

Figure 4.- Continued.

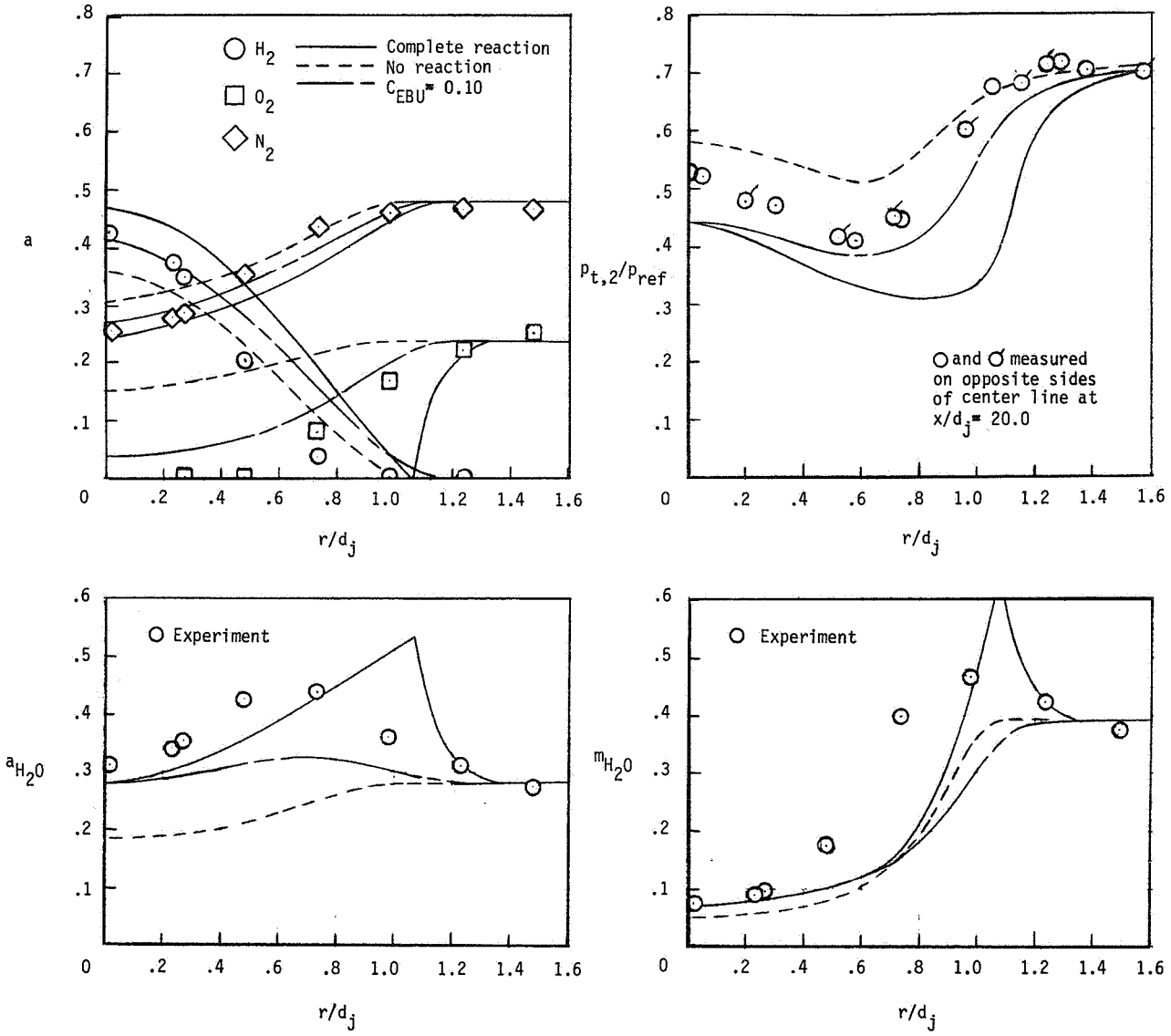

(c) $x/d_j = 21.7$ except for $p_{t,2}/p_{ref}$.

Figure 4.- Continued.

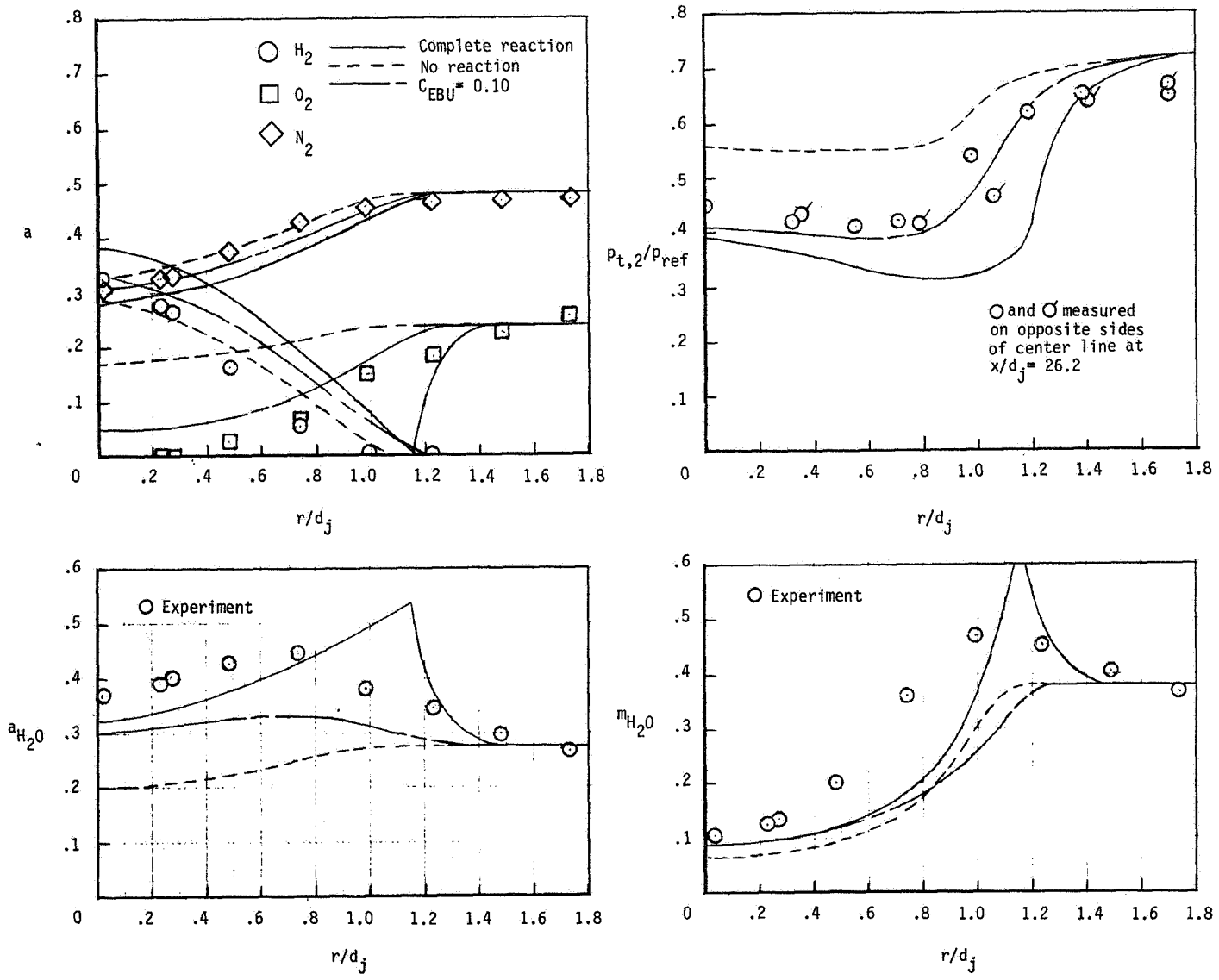

(d) $x/d_j = 27.9$ except for $p_{t,2}/p_{ref}$.

Figure 4.- Concluded.

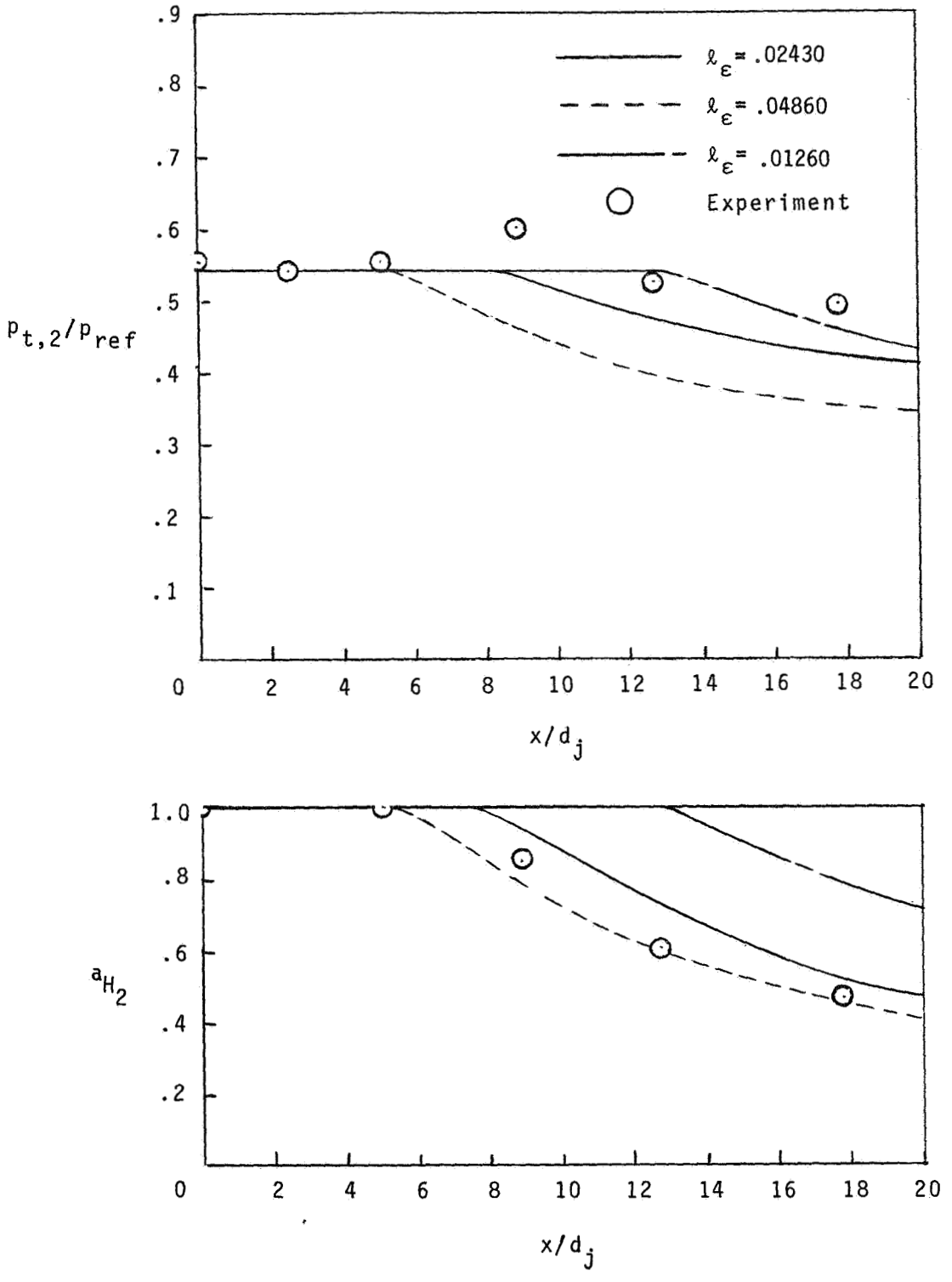

Figure 5.- Axial variation of pitot pressure and hydrogen mass fraction on the center line for case 2. C_{EBU} = 0.05. (H_2 in jet; vitiated air outside.)

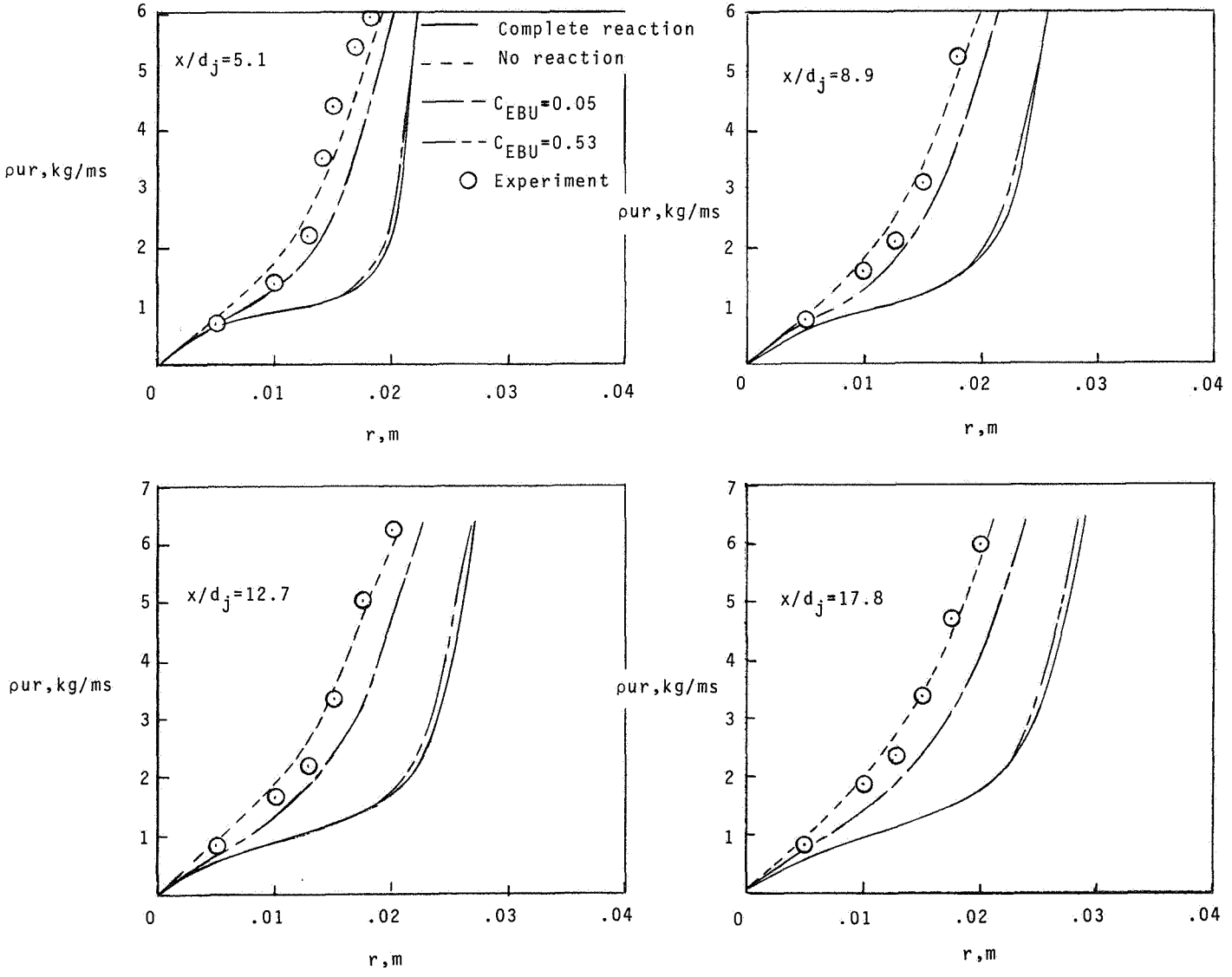

Figure 6.- Distribution of mass flow for case 2. (H_2 in jet; vitiated air outside.)

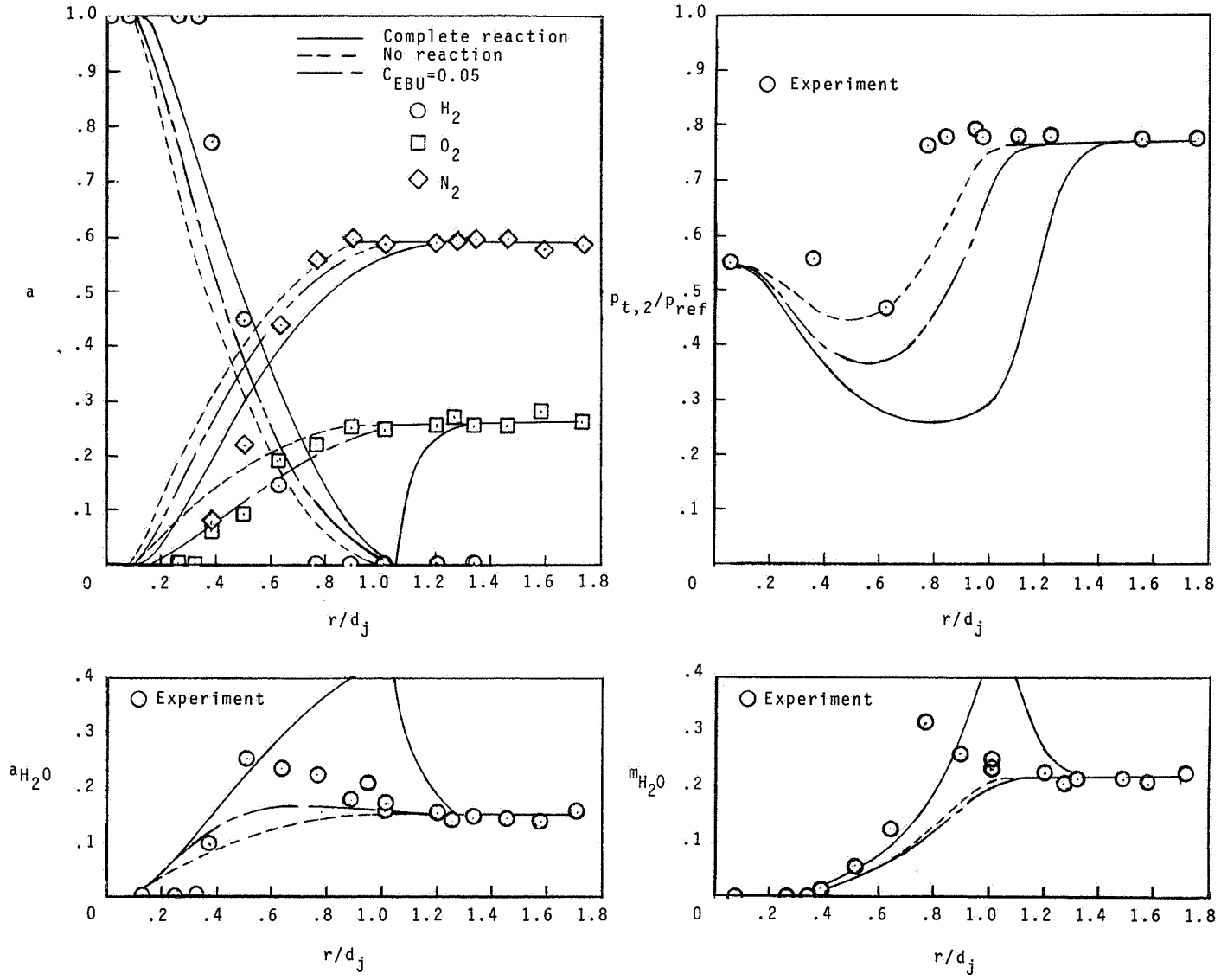

(a) x/d_j = 5.16.

Figure 7.- Profiles of composition and pitot pressure for case 2. (H_2 in jet; vitiated air outside.)

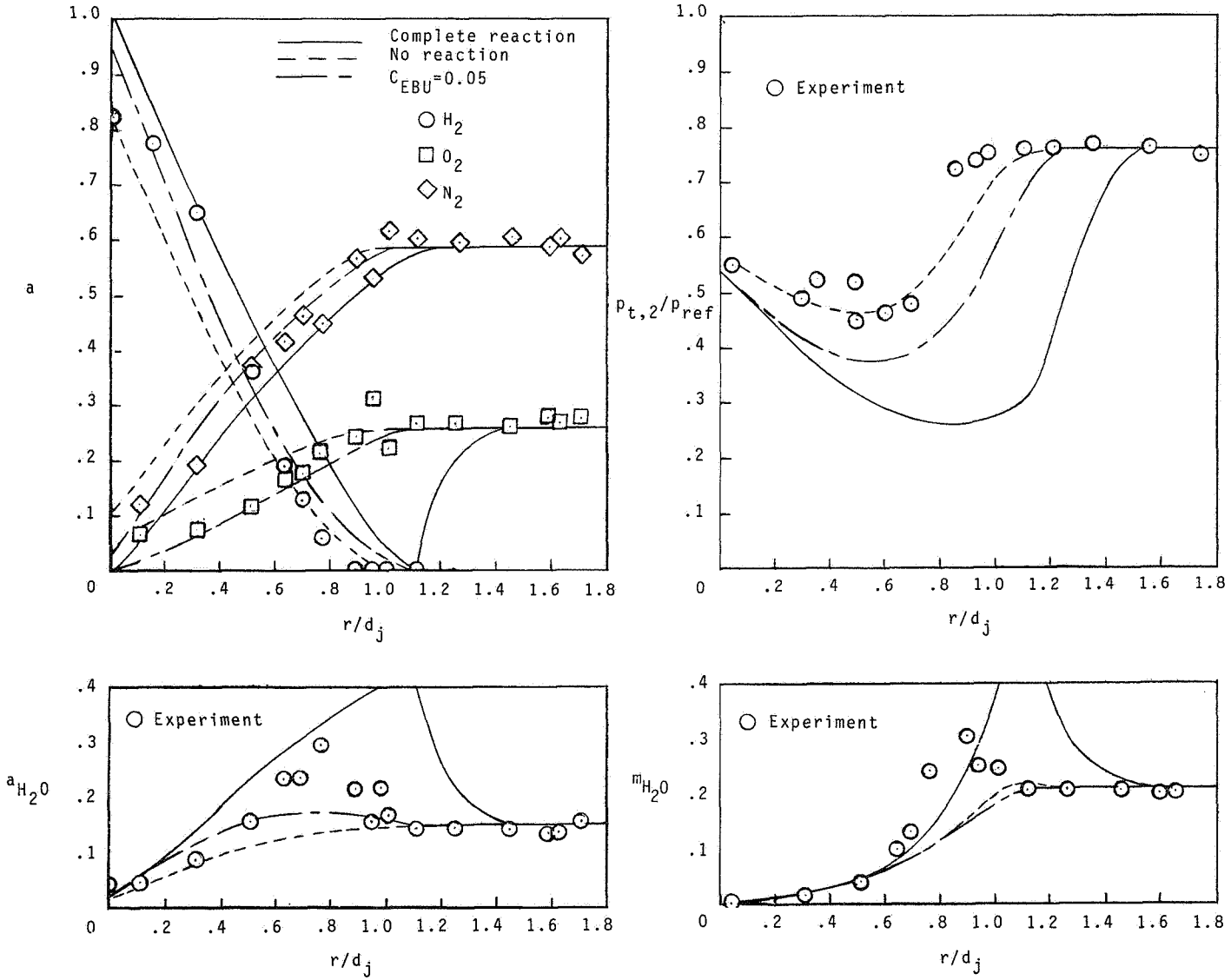

(b) x/d_j = 8.90.

Figure 7.- Continued.

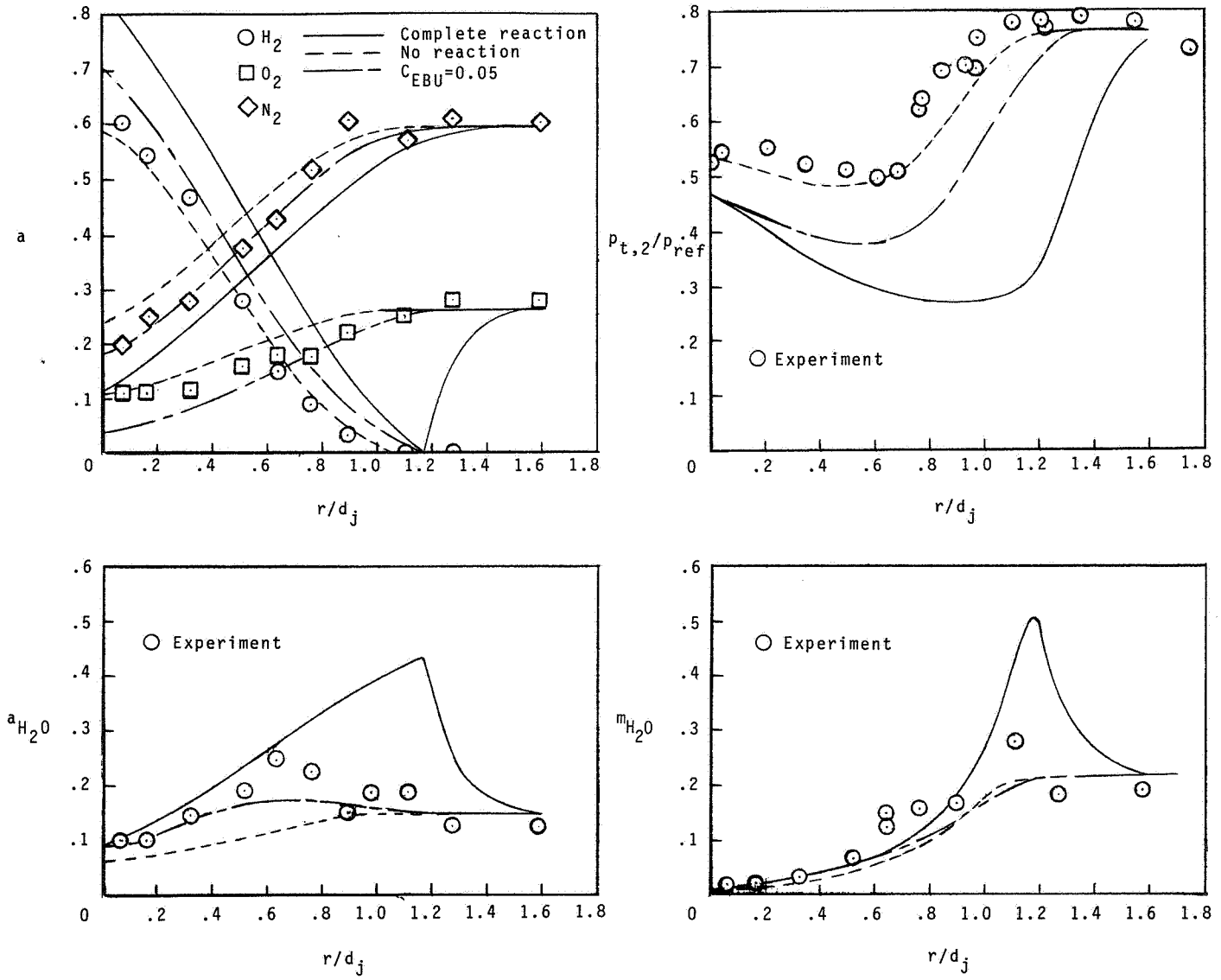

(c) $x/d_j = 12.9$.

Figure 7.- Continued.

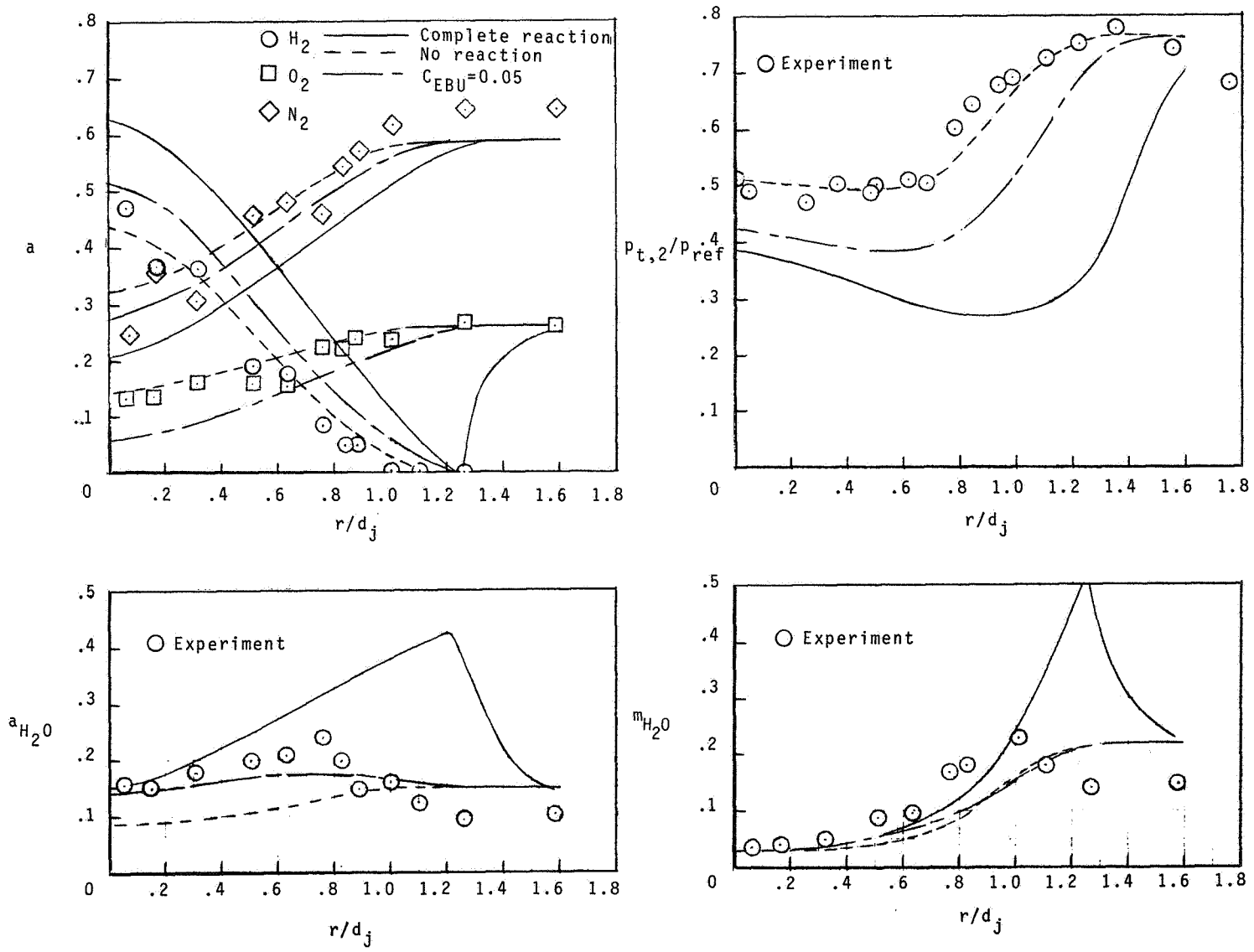

(d) $x/d_j = 17.8$.

Figure 7.- Concluded.

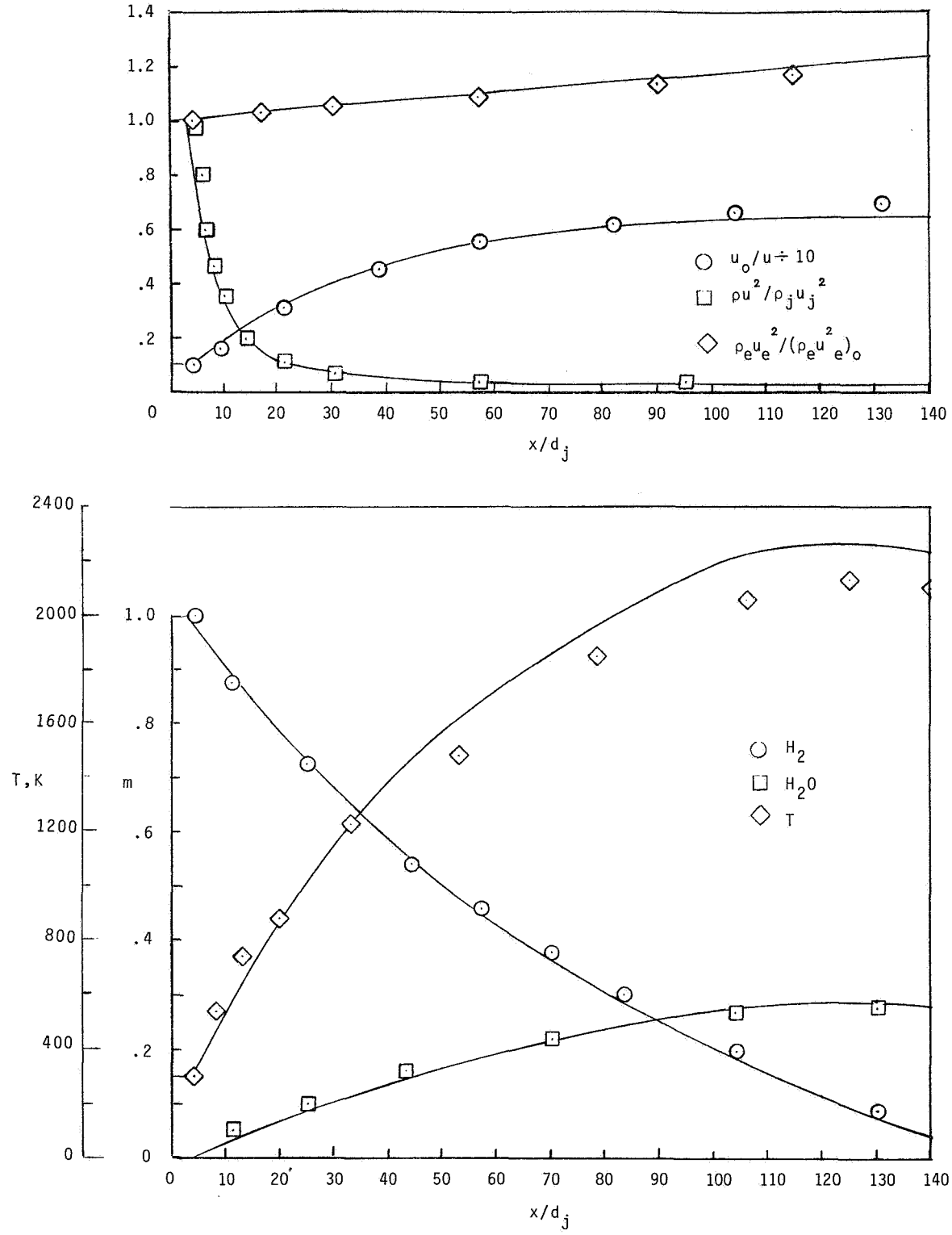

Figure 8.- Axial variation of properties for case 3. Velocity ratio 10 to 1. (H_2 in jet; air outside.)

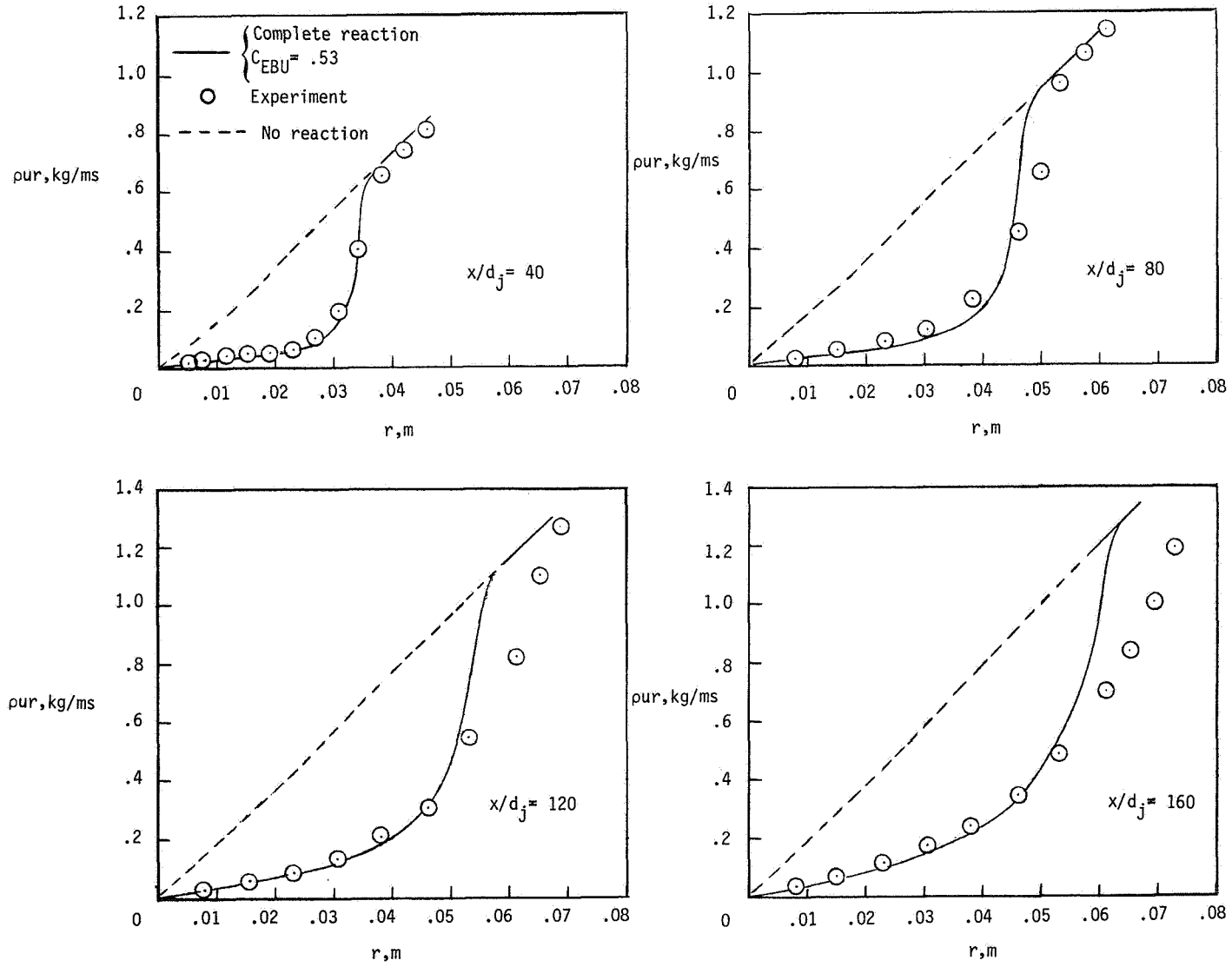

Figure 9.- Distribution of mass flow for case 3. (H_2 in jet; air outside.)

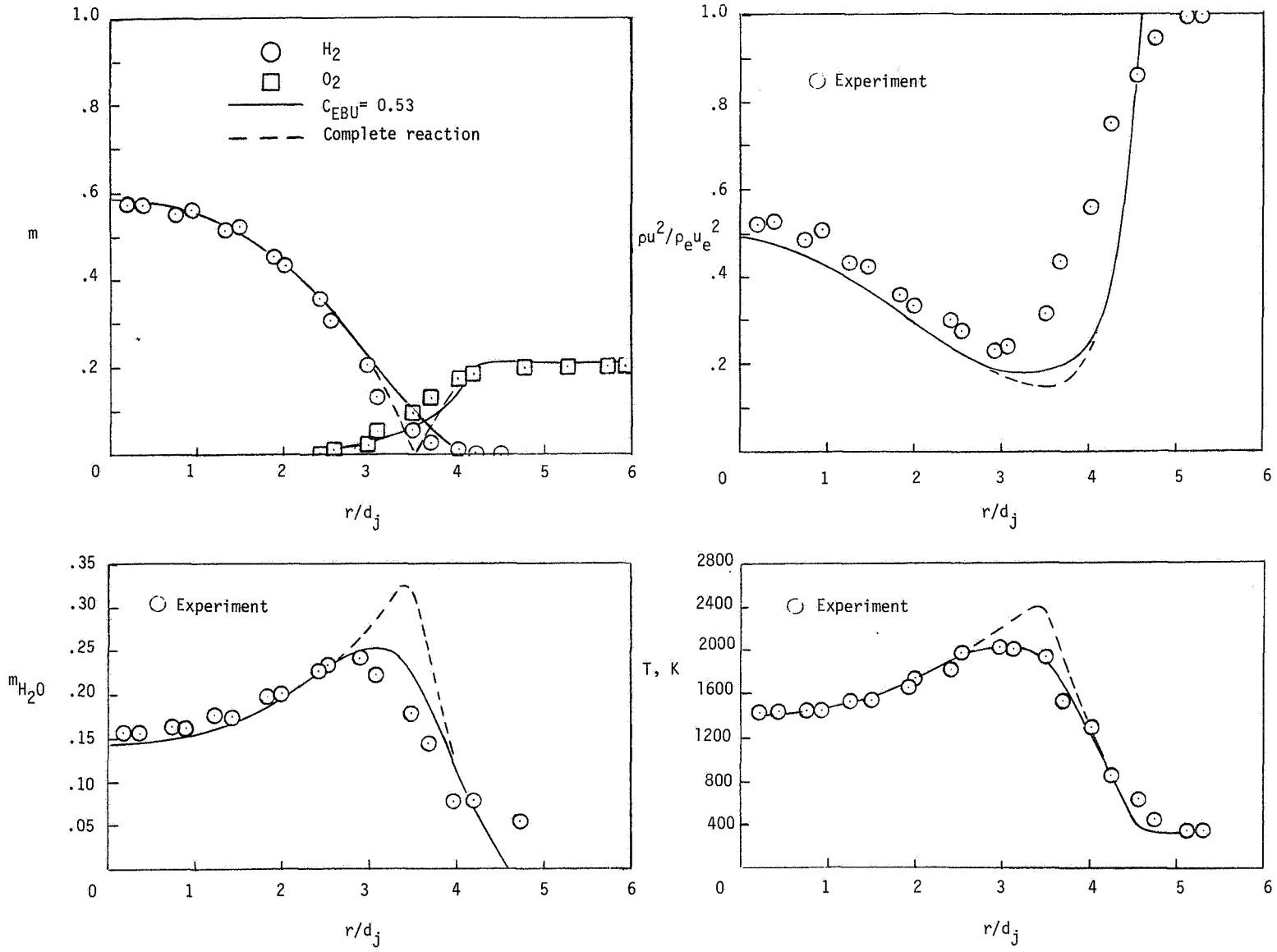

(a) $x/d_j = 40.$

Figure 10.- Profile of temperature, composition, and dynamic pressure for case 3. (H_2 in jet; air outside.)

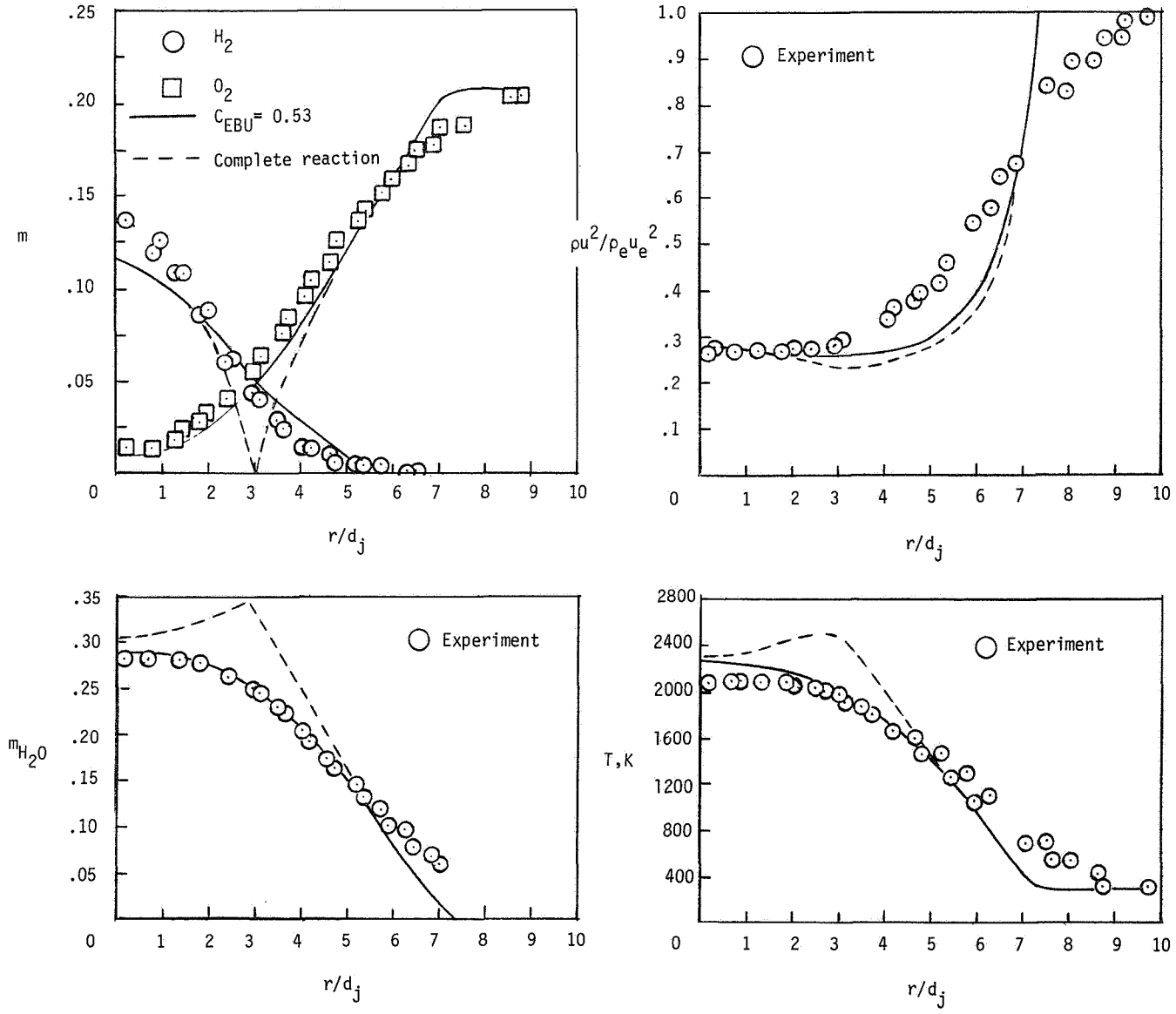

(b) x/d_j = 120.

Figure 10.- Concluded.

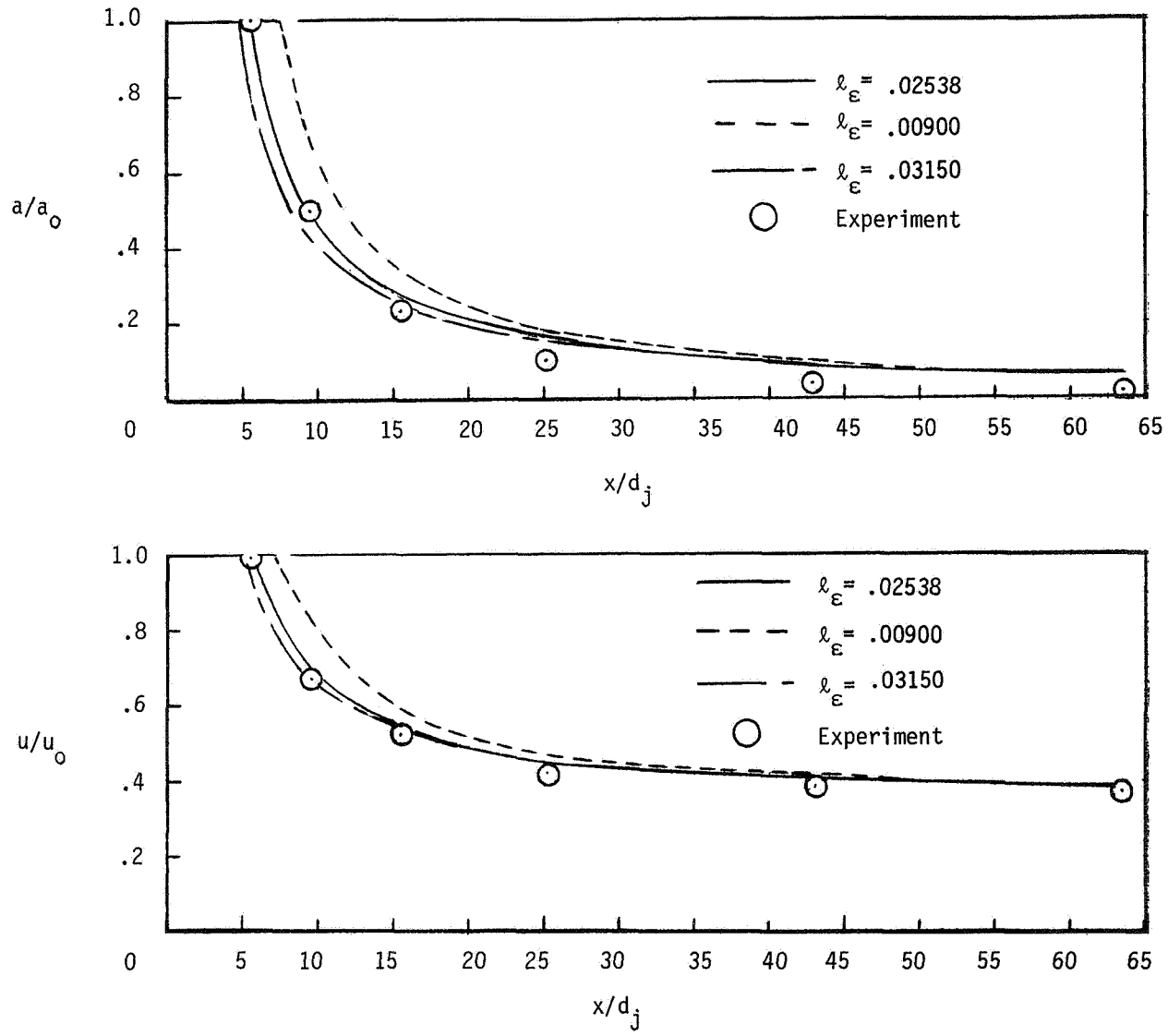

Figure 11.- Variation of properties on the center line for case 4. (H_2 in jet; air outside. There was no chemical reaction in this experiment.)

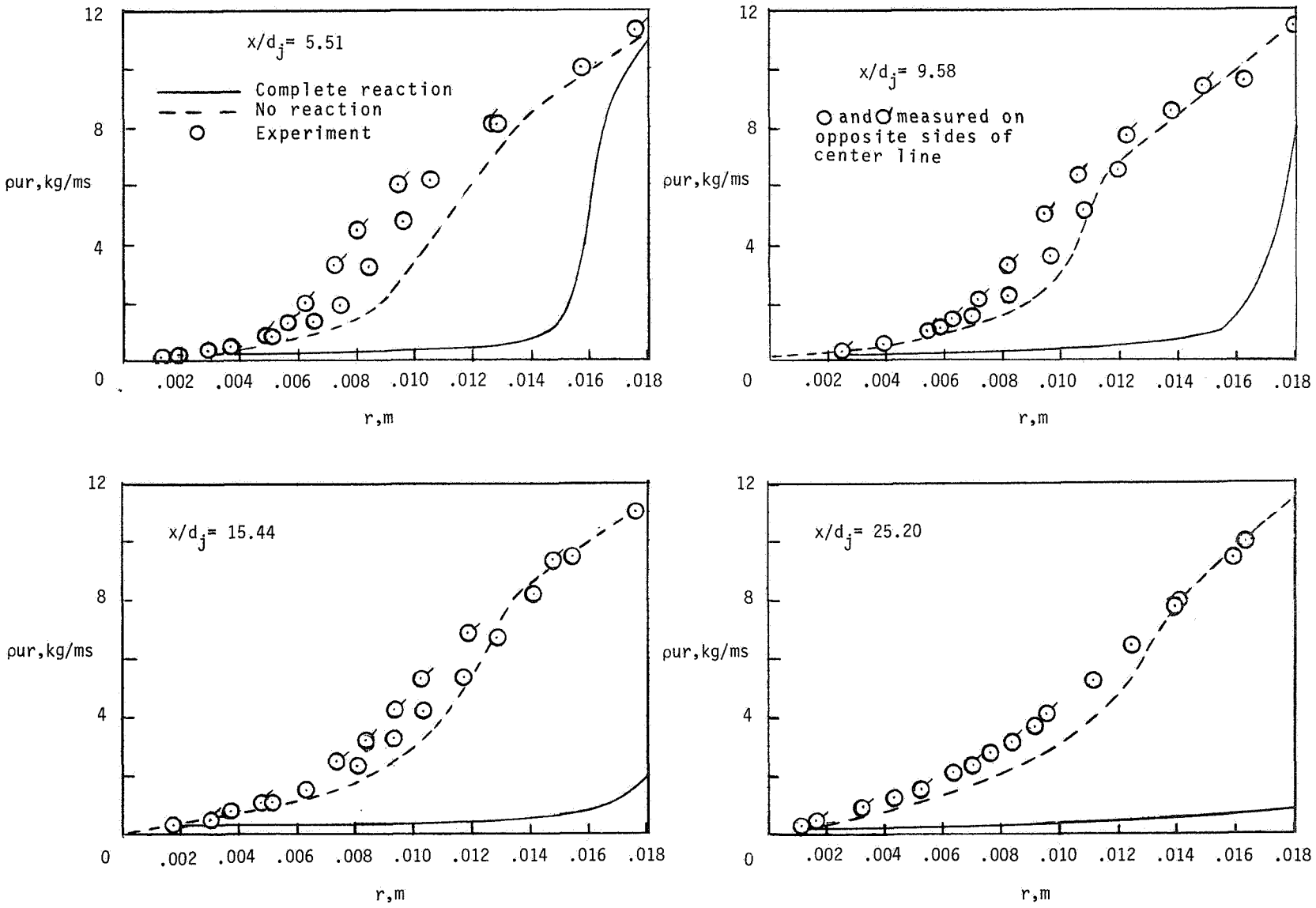

Figure 12.- Distribution of mass flow for case 4. (H_2 in jet; air outside.)

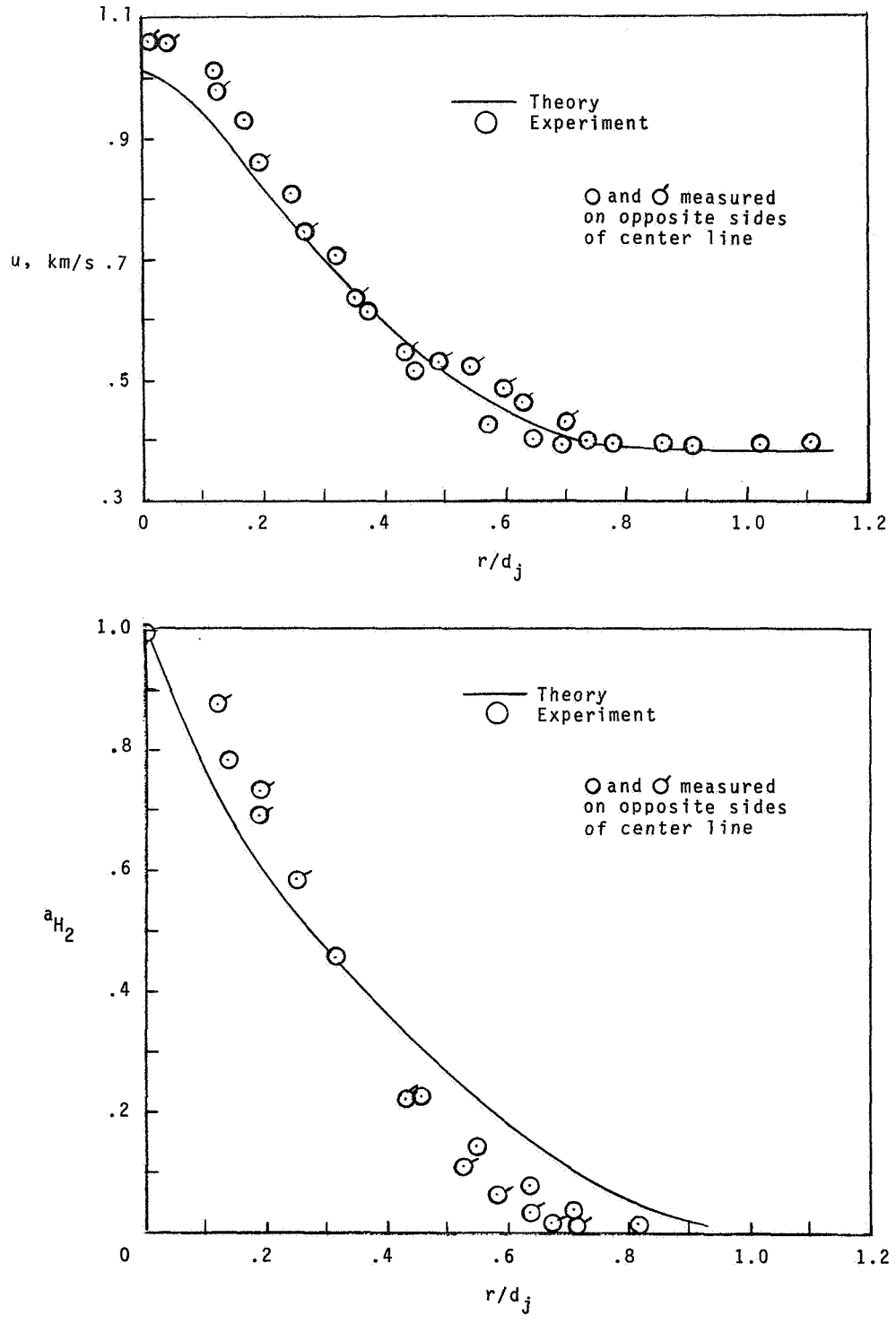

(a) $x/d_j = 5.51$.

Figure 13.- Profiles of velocity and hydrogen mass fraction for case 4. H_2 in jet; air outside.)

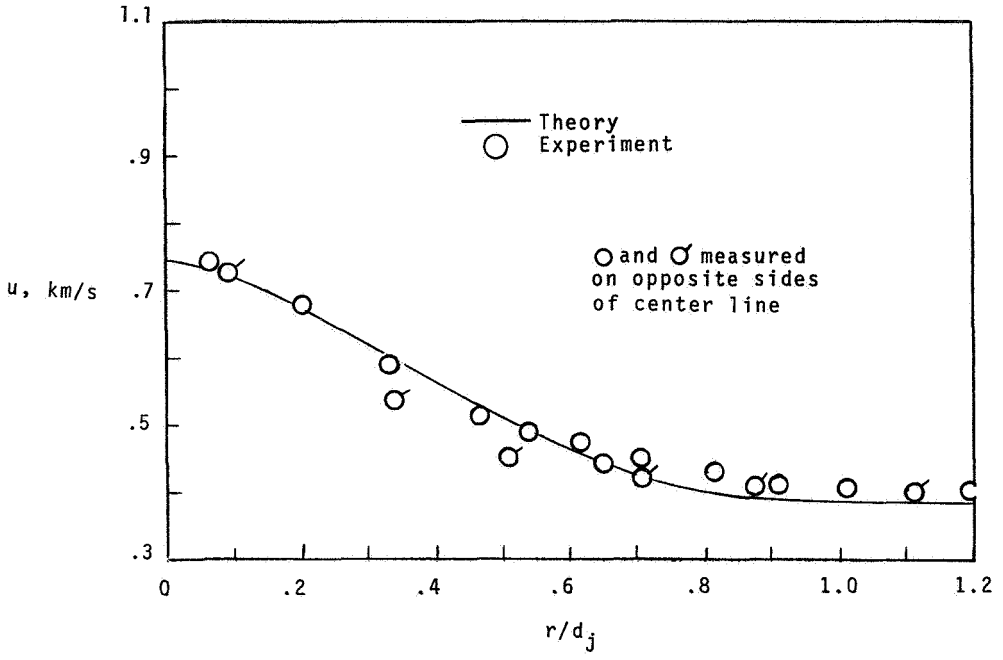

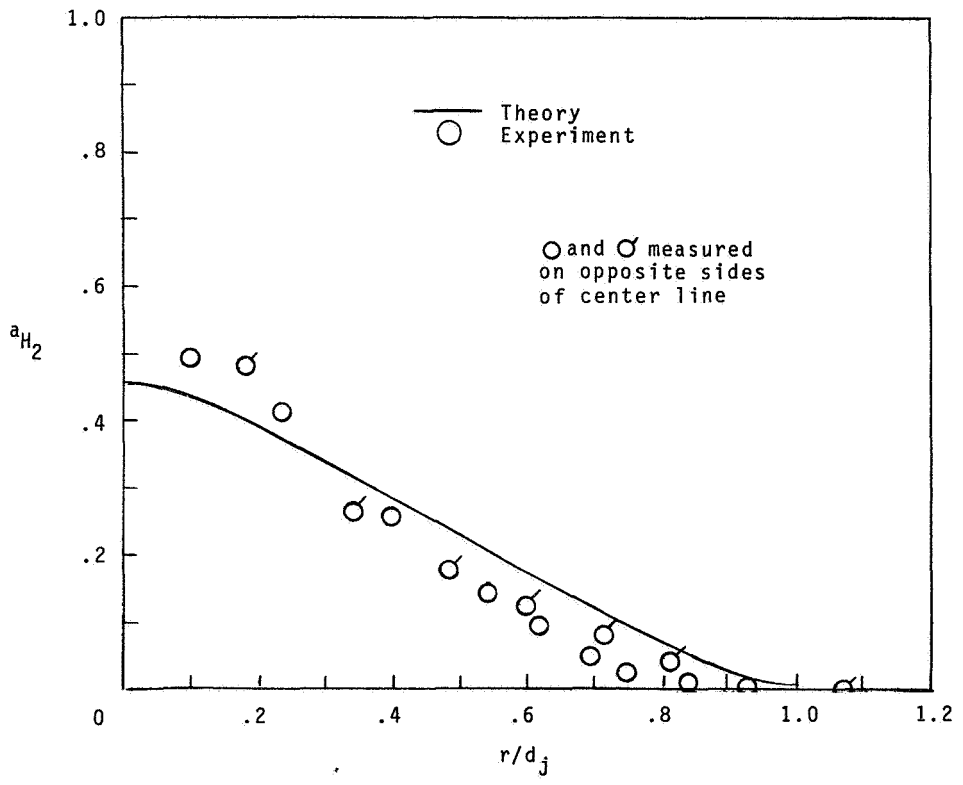

(b) $x/d_j = 9.58$.

Figure 13.- Continued.

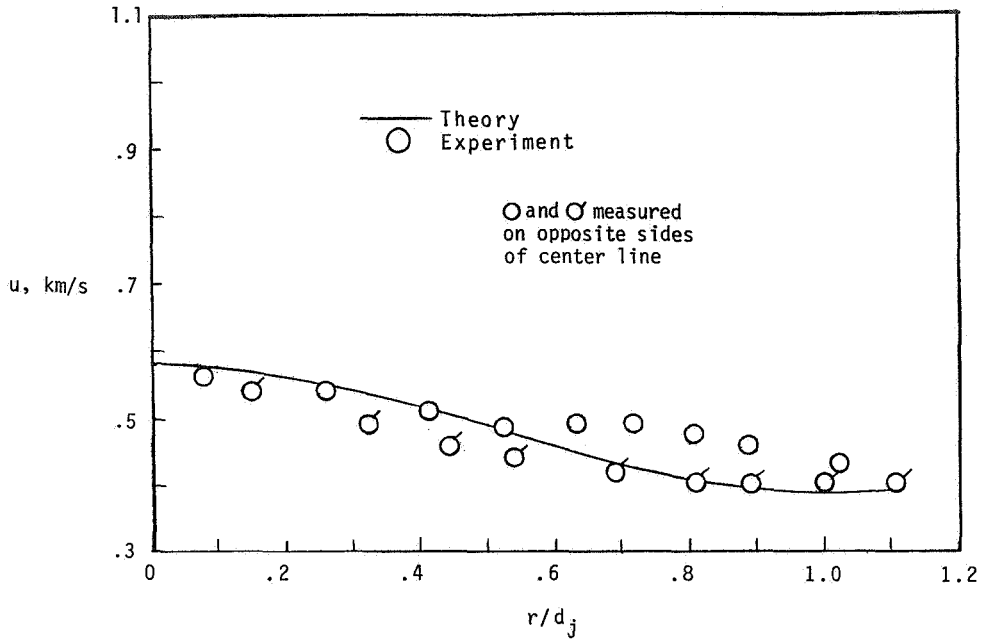

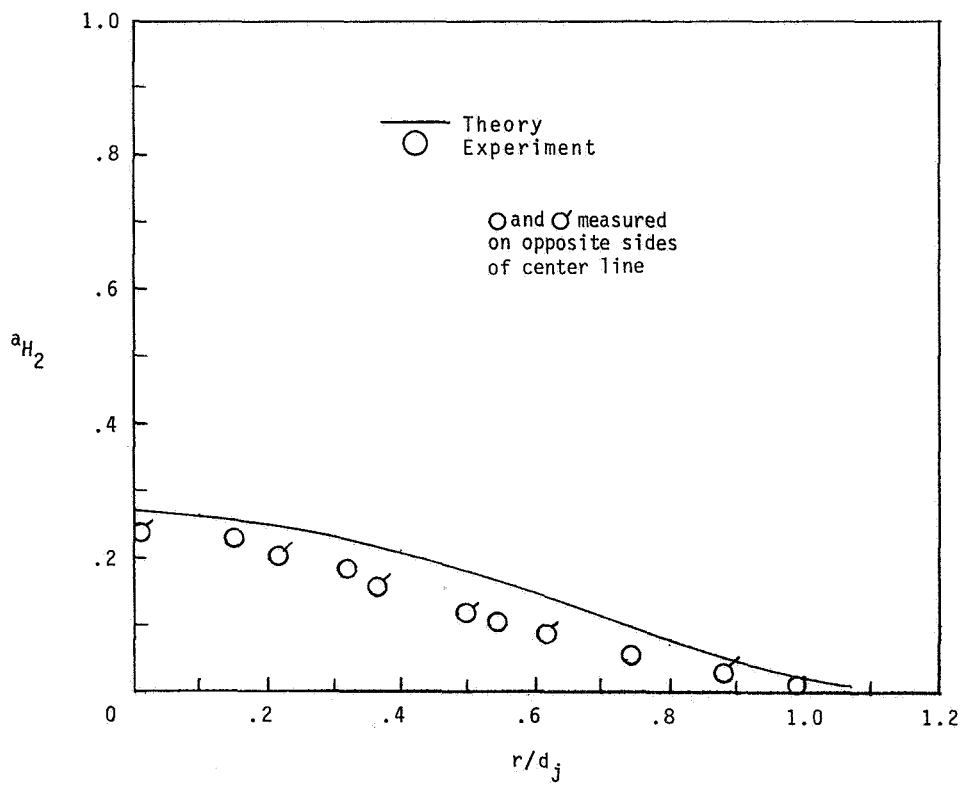

(c) $x/d_j = 15.44$.

Figure 13.- Continued.

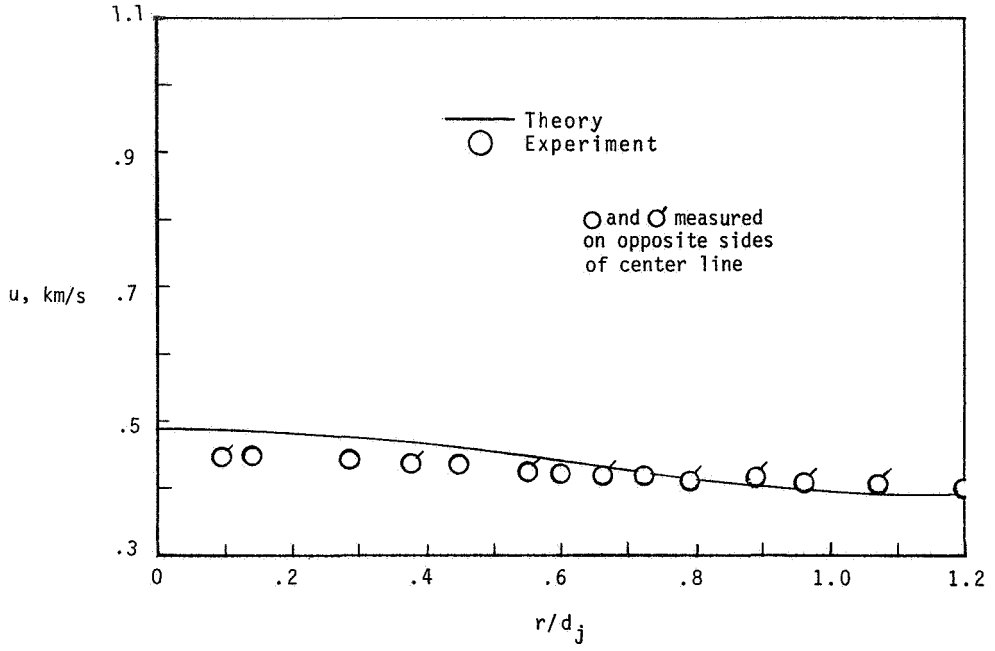

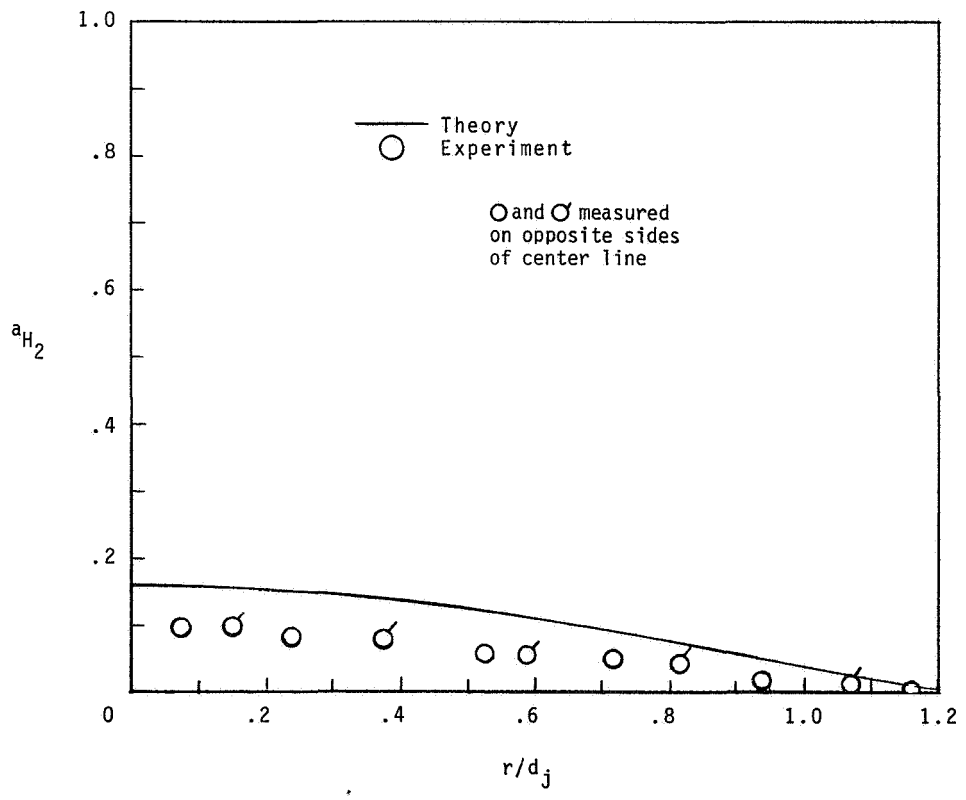

(d) $x/d_j = 25.2$.

Figure 13.- Concluded.

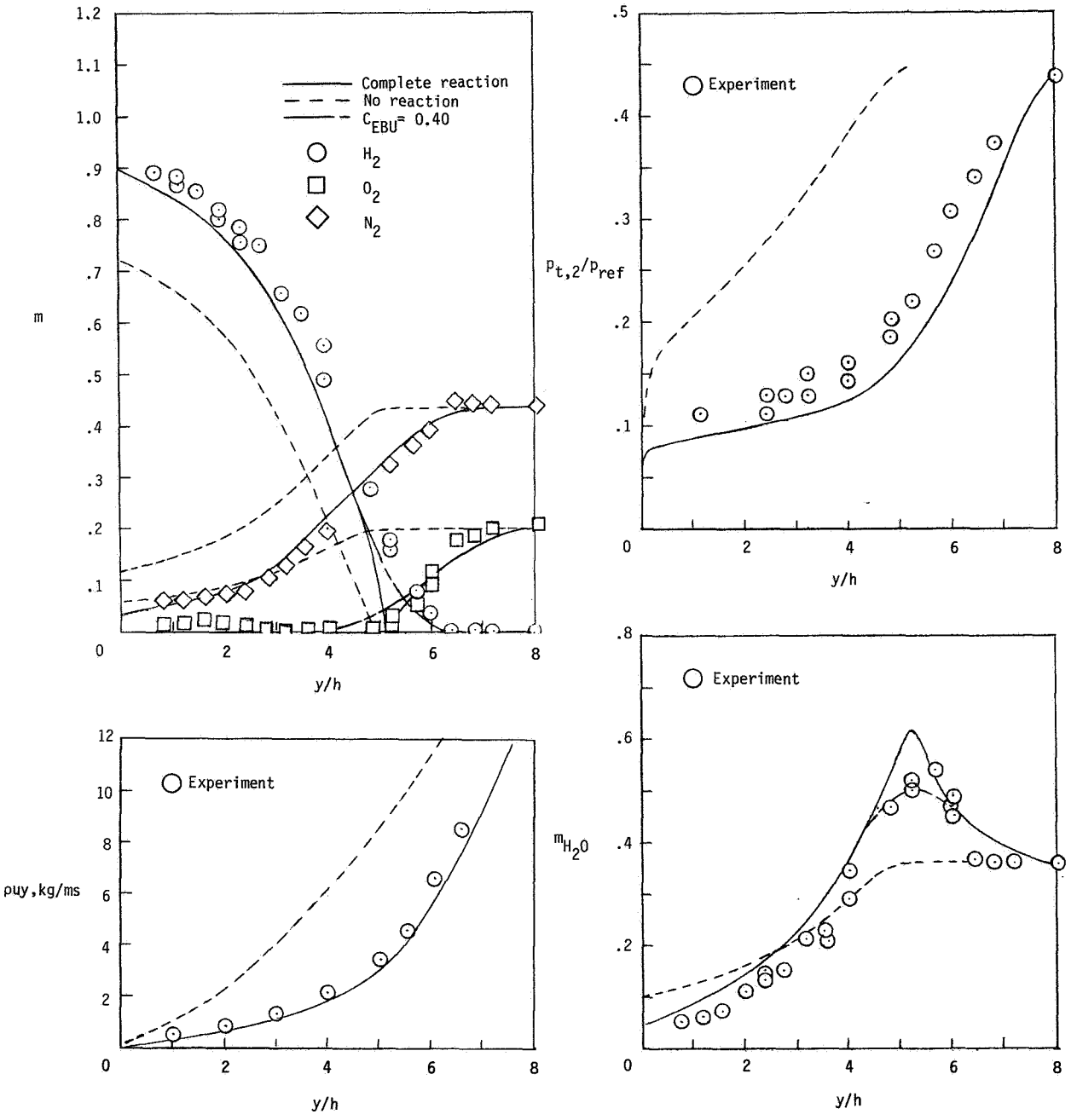

Figure 14.- Profiles of composition, pitot pressure, and mass flow for case 5 at x/h = 89. (H_2 in jet; vitiated air outside.)

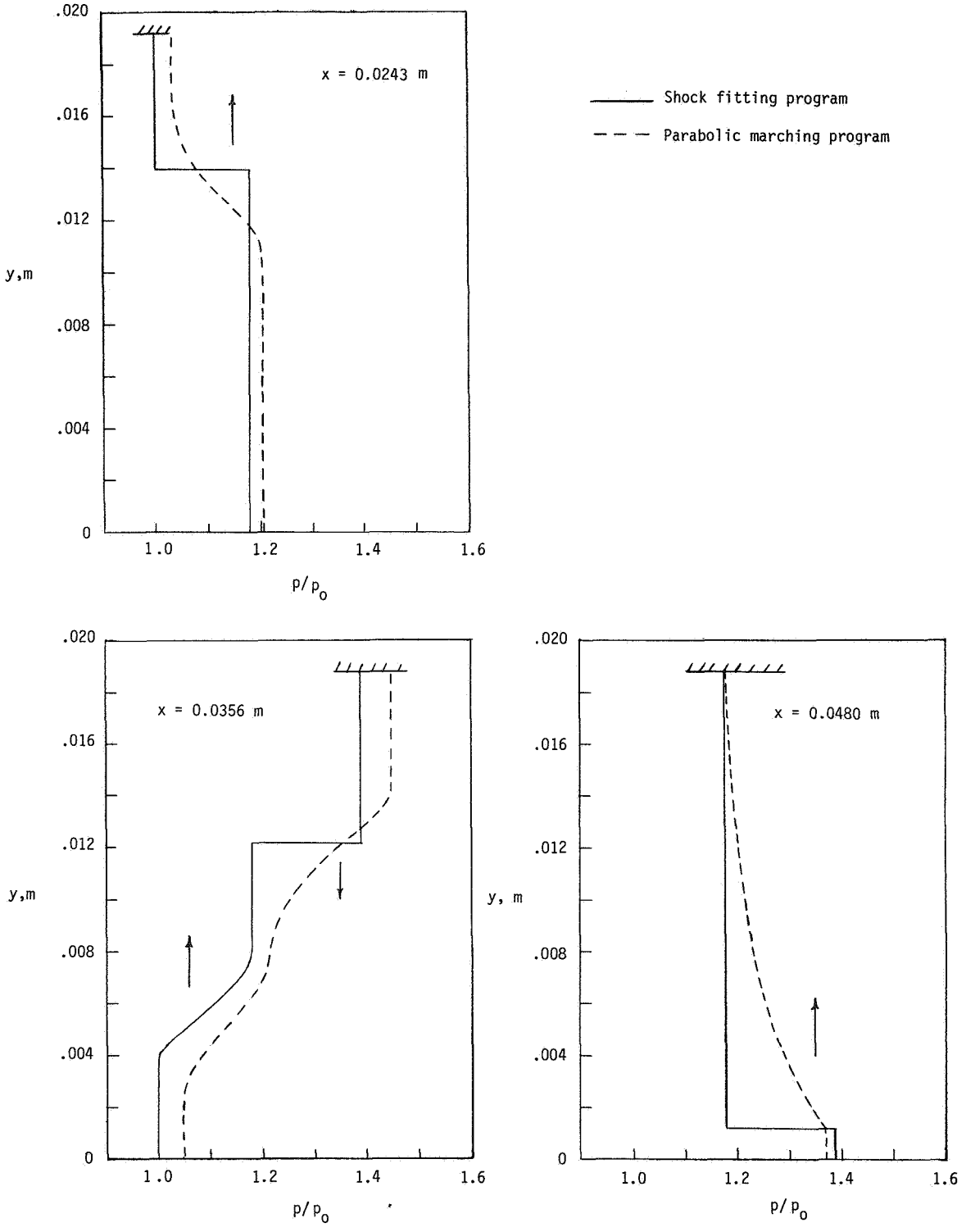

(a) Profiles at x = 0.243 m, x = 0.0356 m, and x = 0.0480 m.

Figure 15.- Pressure distributions for test case 6.

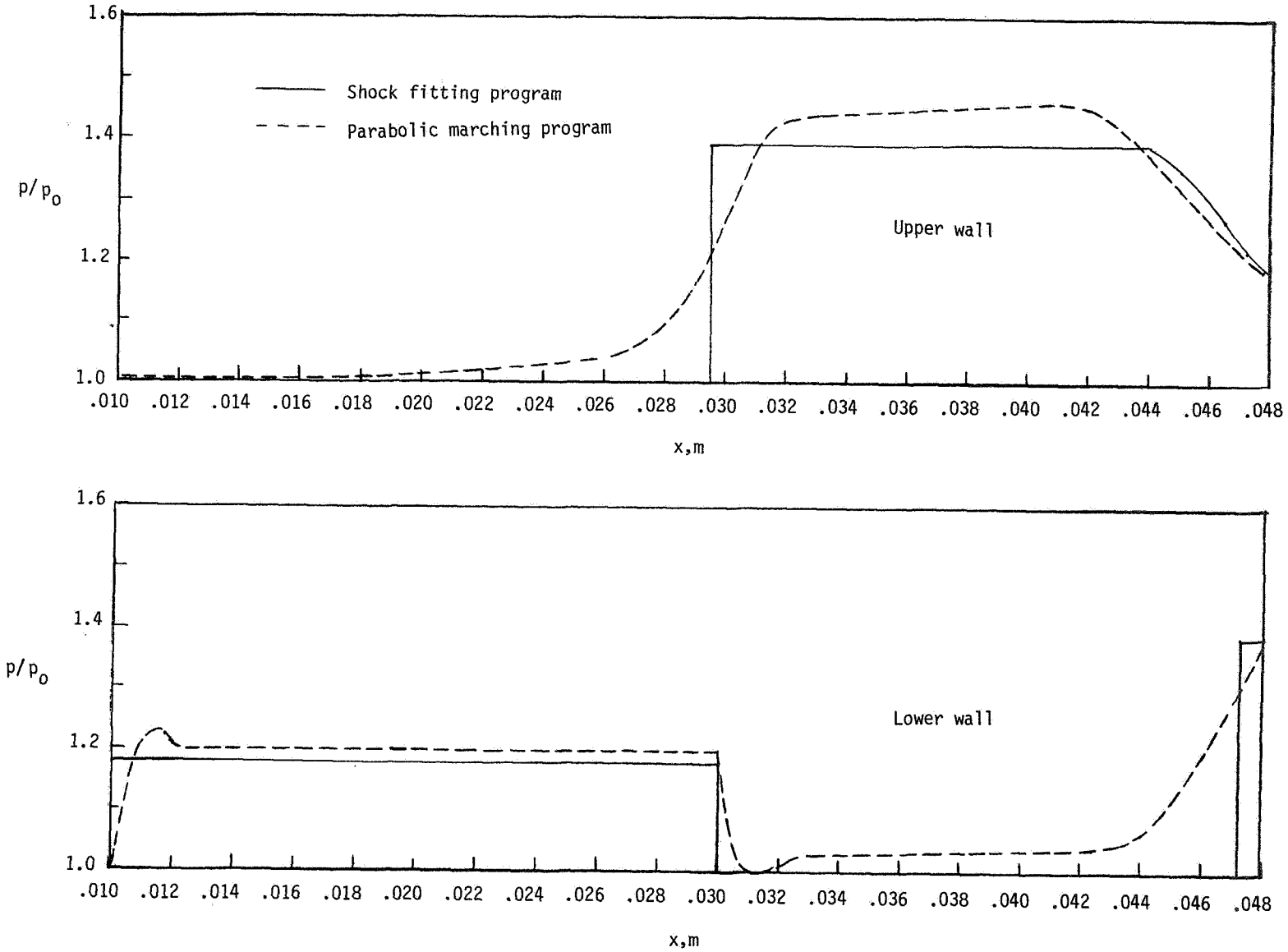

(b) Wall pressures.

Figure 15.- Concluded.

1. Report No.	2. Government Accession No.	3. Recipient's Catalog No.
NASA TP-1169		

4. Title and Subtitle	5. Report Date
APPLICATION OF A TWO-DIMENSIONAL PARABOLIC COMPUTER PROGRAM TO PREDICTION OF TURBULENT REACTING FLOWS	March 1978
	6. Performing Organization Code
7. Author(s) John S. Evans, Charles J. Schexnayder, Jr., and H. L. Beach, Jr.	8. Performing Organization Report No. L-11951
9. Performing Organization Name and Address NASA Langley Research Center Hampton, VA 23665	10. Work Unit No. 505-05-43-01
	11. Contract or Grant No.
12. Sponsoring Agency Name and Address National Aeronautics and Space Administration Washington, DC 20546	13. Type of Report and Period Covered Technical Paper
	14. Sponsoring Agency Code

15. Supplementary Notes

16. Abstract

The capabilities of a computer program obtained from the Spalding group of the Imperial College (London) and further developed by NASA are explored, and computed results are compared with data. The comparisons are restricted to two-dimensional (2-D) flows. Subsonic and supersonic flows, ducted and nonducted, reacting and nonreacting, are considered. Evaluation of models used for turbulence and chemical reaction form an important part of the study. Constants in the $k - \varepsilon$ turbulence model, which produces mixing in good agreement with data, are the same for all calculations, but good initial profiles of turbulence kinetic energy k and dissipation rate of turbulence kinetic energy ε are necessary to obtain satisfactory results. Since calculated results in agreement with the data can be obtained only by adjusting initial profiles in the $k - \varepsilon$ model and a parameter in the reaction model, a true predictive capability is not present. However, the program is useful for interpreting and extrapolating the results of experiments. Experimental data were largely drawn from the literature, but new data are reported for coaxial injection at matched pressure (1 atm or 101.3 kPa) of a cold, Mach 2, hydrogen jet into a hot, Mach 2, vitiated airstream. Profiles of pitot pressure and gas composition obtained from water-cooled probes are reported and compared with theoretical results.

17. Key Words (Suggested by Author(s))	18. Distribution Statement
Turbulent reacting flows Parabolic computer program	Unclassified - Unlimited Subject Category 34

19. Security Classif. (of this report)	20. Security Classif. (of this page)	21. No. of Pages	22. Price*
Unclassified	Unclassified	56	$5.25

* For sale by the National Technical Information Service, Springfield, Virginia 22161

NASA-Langley, 1978

National Aeronautics and
Space Administration

Washington, D.C.
20546

Official Business
Penalty for Private Use, $300

THIRD-CLASS BULK RATE

Postage and Fees Paid
National Aeronautics and
Space Administration
NASA-451

U.S.MAIL

NASA

POSTMASTER: If Undeliverable (Section 158 Postal Manual) Do Not Return